

# Subglacial lakes dynamics

Rotating mixed Rayleigh–Bénard–Horizontal Convection

adrien.villaret

July 2022

## Acknowledgments

I would like to express my deepest gratitude to Louis Couston, my internship master without whom nothing would have been possible, for his patience, advices and his invaluable feedback. I am also deeply indebted to Benjamin Favier for his precious help with Nek5000 and great knowledge of Wall Modes. I would like to thank the PSMN (Pôle Scientifique de Modélisation Numérique) of ENS Lyon for letting me use intensively their computational resources.

I am also thankful to Corentin Prados and Clara Montagnon for sharing my office and being a great company during this internship. Special thanks also to Jason Reneuve for presenting the progress of his work and sharing my back problems. I have to thanks Armelle and Emmanuelle for their welcome at Lyon and their precious help with my different problems. Finally I would like to thank Pauline for being such a great friend and moral support in this big city of Lyon.

## Abstract

Subglacial lakes are very difficult to access and are subject to extreme conditions, similar to what can be found on exoplanets, but life forms have nevertheless been found there, making them particularly interesting for astrobiologists. However, due to their difficulty of access, little is known about the flows in these lakes. A recent study has identified a dominant dynamic, the Rayleigh-Bénard convection, among two possible types of convections, the Horizontal Convection being the second, using numerical simulations in two dimensions. However, this study did not take into account the effect of the Earth's rotation on the competition between these two dynamics.

In this report, we therefore study the influence of rotation on the transition between Rayleigh-Bénard and Horizontal Convection with three-dimensional simulations of confined domains representing subglacial lakes. We start by simulating the two convections separately, with and without rotation, to compare these preliminary results with the literature. Then we mix the two dynamics and study the transition from pure Rayleigh-Bénard to pure Horizontal convection under rotation of different intensity. Our simulations show that rotation has the effect of delaying the transition from Rayleigh-Bénard to Horizontal Convection. Our results therefore confirm the results of the previous study on the fact that Rayleigh-Bénard convection dominates in subglacial lakes.

# Contents

<b>1</b>	<b>Introduction</b>	<b>4</b>
<b>2</b>	<b>Dimensionless Boussinesq equations with the coriolis force</b>	<b>6</b>
2.1	The Boussinesq approximation . . . . .	6
2.2	Dimensionless variables . . . . .	6
2.3	Introductions of the parameters of our problem . . . . .	7
2.4	Implementation of the equations in Nek5000 . . . . .	8
<b>3</b>	<b>Problem representation</b>	<b>8</b>
3.1	Representation . . . . .	8
3.2	Boundary conditions . . . . .	10
3.3	Initial condition . . . . .	11
3.4	Implementation in Nek5000 . . . . .	11
<b>4</b>	<b>Pure Rayleigh-Bénard and Horizontal convection</b>	<b>12</b>
4.1	Without rotation . . . . .	12
4.1.1	Rayleigh-Bénard convection . . . . .	12
4.1.2	Horizontal convection . . . . .	16
4.2	With rotation . . . . .	20
4.2.1	Rayleigh-Bénard convection . . . . .	20
4.2.2	Horizontal Convection . . . . .	27
<b>5</b>	<b>Competition between rotating Rayleigh-Bénard and Horizontal convection</b>	<b>33</b>
5.1	Evolution of the Nusselt numbers . . . . .	33
5.2	Evolution of the temperature profile . . . . .	34
5.3	Evolution of the Reynolds numbers . . . . .	35
5.4	Visualization . . . . .	36
<b>6</b>	<b>Conclusion</b>	<b>40</b>
6.1	Effect of rotation on the transition . . . . .	40
6.2	Possible further research . . . . .	40
<b>A</b>	<b>Effect of the Prandtl number</b>	<b>43</b>
<b>B</b>	<b>Dimensionless numbers</b>	<b>43</b>
B.1	Rayleigh numbers . . . . .	44
B.2	Ekman numbers . . . . .	44
B.3	Nusselt number . . . . .	45

# 1 Introduction

Subglacial lakes, such as lake CECS or lake Vostok in Antarctica, are lakes of freshwater that are found bellow ice sheets, mainly in Antarctica but also in Greenland and Iceland. These lakes (almost 400 have been discovered to this day) contain an important part of Earth freshwater reserve (around 15%), but their main scientific interest lies in astrobiology. Indeed, isolated from the earth atmosphere, under heavy pressure from the three kilometres deep in average icesheet above them and at near  $0^{\circ}\text{C}$  temperature, their conditions approach the ones that can be found on icy exoplanet.

Despite this hostile environment, some of them are known to host extremophilic microbes that live without the energy from the sun, from their interaction with the sediments, the water, and the ice. These inhabitants raise the interest of astrobiologist, in the search for extra-terrestrial life, and drilling have been made to reach these lakes, and more are planned.

In this context, it is interesting to study the dynamics of these subglacial lakes, to determine locations favourable to life and guide the drilling through the icesheet. These lakes have two driving forces, that results in two classical convections. The first energy source is the geothermal heating that occurs at the bottom of the lake. This destabilizes the fluid and, if enough energy is injected, initiates Rayleigh-Bénard convection (RB convection).

The second energy source is as temperature gradient at the top of the lakes. The icesheets covering the lakes have inequal depths, typically getting thinner as they diverge from the center of the ice sheet. This difference in ice height results in difference in pressure which, since the interface between ice and water is at the fusion temperature, which depends on the pressure, results in a temperature difference. The temperature fluctuations considered are very small, but, along kilometres of icesheet, are sufficient to initiate Horizontal Convection (HC), a second classical type of convection. The question is then to determine which of these two convections dominates the dynamics of subglacial lakes.

[1] has already tackle this subject, studying the transition from RB to HC in two dimensions simulations. They have identified a parameter,  $\Lambda$ , that compares the heat flux of HC to the heat flux of RB convection, which most clearly controls whether HC or RB convection is obtained in the lake. They found that the transition occurs at  $\Lambda = 10^{-2}$  and concluded that RB convection dominates in subglacial lakes, since their  $\Lambda$  are much smaller than  $\Lambda = 10^{-2}$ .

Our purpose is to extend their work by considering the rotation of the planet and studying its effect on the transition from RB to HC. RB convection has been extensively studied in the literature. [2] studies in depth RB convection, with and without rotation. It calculates the critical Rayleigh number at which the convection starts without rotation, with free or no-slip boundary conditions for the velocity and no side walls, and then with rotation, whose importance on the dynamics is encapsulated in the so-called Ekman number. In the absence of rotation, [3] describes its dynamics and the importance of the boundary layers, discusses the effect of the viscosity and aspect ratio and proposes scalings for the heat transfer and the kinetic energy with the most important control parameter, which is the Rayleigh number  $Ra$ .

Considering the effect of rotation on RB, [4], using heat transfer as a criterion to determine the influence of rotation, proposes a phase diagram in  $(Ra, Ek)$  parameter space, where  $Ek$  is the Ekman number. [5] describes the evolution of the heat transfer with rotation (through the Ekman number) and energy input (through the  $Ra$  number), comparing results between simulations and experiments. [6] focuses on a particular aspect of confined rotating RB convection, the Wall Modes. He describes this particular convection and its strength depending on the Ekman number and the Rayleigh number.

HC is also well-documented in the literature. [7] describes the structure of the flow without rotation, distinguishing different convection regimes as the energy input, estimated from a horizontal Rayleigh number  $Ra_L$ , varies. [8] and [9] focus on the effect of rotation on HC. They provide a criterion,  $Q$ , to evaluate the influence of rotation over the flow and propose scalings for the heat transfer depending on rotation and energy input (through horizontal Ekman and Rayleigh number  $Ek_L$  and  $Ra_L$ ).

The effect of the shape of the container on RB and HC is also a documented subject. [10] and [11] explore the effects of the aspect ratio, and of the shape of the container for the second one, on RB convection, studying the critical Rayleigh number at which the convection starts. For HC, [12] has studied the effect of the aspect number on the convection and the scaling of the Nusselt number with the Rayleigh number.

We have to precise that if these previous works are an excellent starting point for our work and help us understand our results, we can not just take their results for benchmarking our mixed RB and HC. Indeed, the choice of domain geometry, size, as well as the choice of governing equations and  $Pr$  vary between studies and influence the dynamics in sometimes non-negligible and not-fully-understood ways. Therefore, an important part of our work will be to redo simulations of classical RB and HC separately for our particular setup, which will then serve as references for mixed RBHC.

## 2 Dimensionless Boussinesq equations with the coriolis force

### 2.1 The Boussinesq approximation

The Navier-Stokes equations in their incompressible form, taking into account the Coriolis force and gravity, are:

$$\begin{cases} \rho \frac{D\mathbf{u}}{Dt} = -\nabla p + \mu \Delta \mathbf{u} - 2\rho \boldsymbol{\Omega} \wedge \mathbf{u} + \rho \mathbf{g} \\ \nabla \cdot \mathbf{u} = 0 \\ \frac{DT}{Dt} = \kappa \nabla^2 T. \end{cases} \quad (1)$$

In equation 1, we take  $\kappa$  as the thermal diffusivity of the fluid,  $\mu$  the dynamic viscosity,  $\rho$  the density,  $\mathbf{g}$  the gravity and  $\boldsymbol{\Omega} = -\omega \mathbf{e}_z$  the rotation rate of Earth (it is negative since we are considering lakes in the South Pole and we are making the f-plane approximation).

Then, we make the Boussinesq approximation: variations of the density of the fluid are assumed small, such that they only enter the buoyancy term  $\rho \mathbf{g}$ , which is related to temperature through a linear equation of state. Thus, it is only taken into account as a variation of the gravity force:

$$\begin{cases} \rho \rightarrow \rho_0 \\ \rho \mathbf{g} \rightarrow \rho_0 \mathbf{g} - \rho_0 \alpha \mathbf{g} \delta T \end{cases} \quad (2)$$

where  $\rho_0$  is the mean density,  $\alpha$  the thermal expansion coefficient of the fluid and  $\delta T = T - T_0$  the difference between the local temperature and a reference temperature (that sets  $\rho_0$ ).

The first equation of 1 becomes:

$$\rho_0 \frac{D\mathbf{u}}{Dt} = -\nabla p + \mu \Delta \mathbf{u} - 2\rho_0 \boldsymbol{\Omega} \wedge \mathbf{u} + (1 - \alpha \delta T) \rho_0 \mathbf{g}. \quad (3)$$

### 2.2 Dimensionless variables

We want to non-dimensionalize those equations. We will start by considering a characteristic diffusive time:

$$\tau = \frac{H^2}{\kappa} \quad (4)$$

with  $H$  the characteristic height of the problem (here the height of the box). With these characteristic time and height we can define a characteristic velocity:

$$u_0 = \frac{H}{\tau}. \quad (5)$$

We can rewrite (5) as  $u_0 = \frac{\kappa}{H}$ , the diffusion velocity.

We can now define dimensionless variables:

$$\begin{cases} t = \tau \bar{t} = \frac{H^2}{\kappa} \bar{t} \\ \mathbf{u} = u_0 \bar{\mathbf{u}} \\ x, y, z = H \bar{x}, \bar{y}, \bar{z} \\ \delta T = \Delta T \bar{T} \\ p = p_0 \bar{p} \end{cases} \quad (6)$$

with  $p_0$  a characteristic pressure and  $\Delta T$  a characteristic temperature difference. Since in our problem we impose a heat flux  $F$ , we can link this temperature difference to it with the relation

$$\Delta T = \frac{FH}{k} \quad (7)$$

where  $k$  is the thermal conductivity (this relation comes directly from Fourier's law in thermal conduction). We can also introduce  $f = 2\omega \sin(\text{latitude}) = -2\omega$  the Coriolis frequency.

This give us the following equations (for simplicity we get rid of the overlines):

$$\begin{cases} \frac{\rho_0 u_0 \kappa}{H^2} \frac{D\mathbf{u}}{Dt} = -\frac{p_0}{H} \nabla p + \frac{\mu u_0}{H^2} \Delta \mathbf{u} - \rho_0 u_0 f \mathbf{e}_z \wedge \mathbf{u} - (1 - \alpha \Delta T T) \rho_0 g \mathbf{e}_z \\ \nabla \cdot \mathbf{u} = 0 \\ \frac{\Delta T \kappa}{H^2} \frac{DT}{Dt} = \frac{\kappa \Delta T}{H^2} \nabla^2 T. \end{cases} \quad (8)$$

As  $u_0 = \frac{H}{\tau} = \frac{\kappa}{H}$  and  $\Delta T = \frac{FH}{k}$  we can rewrite 8:

$$\begin{cases} \frac{D\mathbf{u}}{Dt} = -\frac{p_0 H^2}{\rho_0 \kappa^2} \nabla p + \frac{\mu}{\rho_0 \kappa} \Delta \mathbf{u} - \frac{H^2}{\kappa} f \mathbf{e}_z \wedge \mathbf{u} - \frac{(1 - \alpha \frac{FH}{k} T) g H^3}{\kappa^2} \mathbf{e}_z \\ \nabla \cdot \mathbf{u} = 0 \\ \frac{DT}{Dt} = \nabla^2 T. \end{cases} \quad (9)$$

Since  $g$  is the gradient of the gravity potential, we can create a new pressure:

$$\nabla \pi = \nabla \left( \frac{p_0 H^2}{\rho_0 \kappa^2} p + \frac{H^3}{\kappa^2} g z \right). \quad (10)$$

We can also introduce the kinematic viscosity:

$$\nu = \frac{\mu}{\rho_0}. \quad (11)$$

Thus we get:

$$\begin{cases} \frac{D\mathbf{u}}{Dt} = -\nabla \pi + \frac{\nu}{\kappa} \Delta \mathbf{u} - \frac{f H^2}{\kappa} \mathbf{e}_z \wedge \mathbf{u} + \frac{\alpha F g H^4}{\kappa^2 k} T \mathbf{e}_z \\ \nabla \cdot \mathbf{u} = 0 \\ \frac{DT}{Dt} = \nabla^2 T. \end{cases} \quad (12)$$

### 2.3 Introductions of the parameters of our problem

We can start now defining dimensionless numbers that will be characteristic of our flow, with  $Pr$  the Prandtl number,  $Ra$  the Rayleigh number and  $Ek$  the Ekman number:

$$\begin{cases} Pr = \frac{\nu}{\kappa} \\ Ra = \frac{g \alpha F H^4}{\kappa k \nu} \\ Ek = \frac{\nu}{|f| H^2} = -\frac{\nu}{f H^2}. \end{cases} \quad (13)$$

We can note that what we call in this section  $Ra$  will later be called  $Ra_F$ , because a distinction will be made with the Rayleigh numbers  $Ra_T$  and  $Ra_L$ , corresponding respectively to the Rayleigh number for RB convection where the temperature difference is imposed and to the Rayleigh number for HC. The dimensionless equations can then be rewritten as

$$\begin{cases} \frac{D\mathbf{u}}{Dt} = -\nabla\pi + Pr\Delta\mathbf{u} + \frac{Pr}{Ek}\mathbf{e}_z \wedge \mathbf{u} + RaPrT\mathbf{e}_z \\ \nabla \cdot \mathbf{u} = 0 \\ \frac{DT}{Dt} = \nabla^2 T. \end{cases} \quad (14)$$

We can then see that the relative influence of buoyancy, driver of RB and HC, and Coriolis force, that tends to stabilize the system, can be studied in a phase diagram with the variations of the Ekman and Rayleigh number  $Ek$  and  $Ra$  (provided that we fix  $Pr$ ).

## 2.4 Implementation of the equations in Nek5000

The software we will use for our simulations, Nek5000, already includes the basic dimensionless Navier-Stokes equations. Thus, here we only have to add the Coriolis force to the momentum equations in  $x$  and  $y$  and the buoyancy force to the equation in the  $z$  direction, i.e.

$$\mathbf{ff} = RaPrT\mathbf{e}_z + \frac{Pr}{Ek}\mathbf{e}_z \wedge \mathbf{u}. \quad (15)$$

As explained previously, since the lakes are mainly found at the South Pole,  $\boldsymbol{\Omega} = -\omega\mathbf{e}_z$ . Thus we expect to see a deviation to the left due to the Coriolis force.

$$\mathbf{e}_z \wedge \mathbf{u} = \begin{pmatrix} 0 \\ 0 \\ 1 \end{pmatrix} \wedge \begin{pmatrix} u_x \\ u_y \\ u_z \end{pmatrix} = \begin{pmatrix} -u_y \\ u_x \\ 0 \end{pmatrix}. \quad (16)$$

We observe a deviation to the left. The total force is thus:

$$\frac{Pr}{Ek}\mathbf{e}_z \wedge \mathbf{u} = \frac{Pr}{Ek} \begin{pmatrix} -u_y \\ u_x \\ 0 \end{pmatrix}. \quad (17)$$

The force components added to the RHS of the momentum equations in Nek5000 are then:

$$\begin{cases} ffx = -\frac{Pr}{Ek}u_y \\ ffy = \frac{Pr}{Ek}u_x \\ f fz = RaPrT. \end{cases} \quad (18)$$

## 3 Problem representation

### 3.1 Representation

The subglacial lake will be represented in our computation by a box with the dimensions  $L_x$ ,  $L_y$  and  $H$  in the directions  $x$ ,  $y$  and  $z$  respectively (see figure 1). We will non-dimensionalize those lengths by the vertical one ( $H$ ), that we already use to non-dimensionalize in equation (6):

$$\begin{cases} L_x = \overline{L}_x H \\ L_y = \overline{L}_y H \\ H = \overline{H} H. \end{cases} \quad (19)$$

$\overline{L}_x$  corresponding to the width-over-height aspect ratio of the box (in the  $x$  direction, where we have a temperature gradient), we will now also call it  $\Gamma$

$$\Gamma = \overline{L}_x. \quad (20)$$

We will take  $\Gamma = \overline{L_x} = 4$  and  $\overline{L_y} = 1$  in our computations (the value of  $\overline{H}$  is fixed at 1 as we chose H as the characteristic length). The HC, driven by a difference in temperatures, mimics the result of a varying ice thickness. That being said, for simplifications we will consider a flat top, taking only into account the temperature gradient.

Since we want to study the competition between Horizontal Convection and Rayleigh-Bénard convection, we will need a controlling parameter, characterizing the strength of one dynamic in relation to the other. We chose in the following simulations to use:

$$\Lambda = \frac{k\lambda}{F} \quad (21)$$

with  $\lambda$  the temperature gradient along the top boundary, k the thermal conductivity and F the bottom heat flux. This parameter establishes a ratio between horizontal and Rayleigh-Bénard forcing by establishing a ratio between the two different thermal fluxes. We will consider  $\Lambda$  going from 0 (pure Rayleigh-Bénard convection) to 1 (value for which [1] shows that Horizontal convection largely dominates), as well as the corresponding case of  $\Lambda = \infty$  of pure HC (in practice we will always consider a finite  $\Lambda$  but turn off geothermal heating for pure HC simulations).

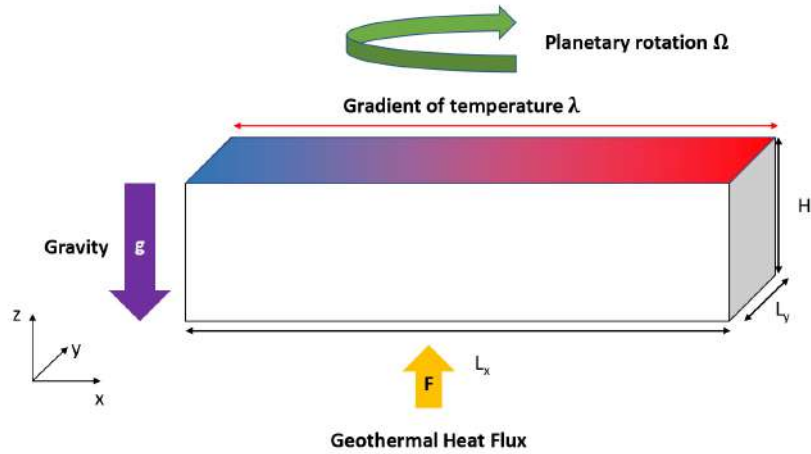


Figure 1: Representation of the the domain and buoyancy sources considered.

### 3.2 Boundary conditions

For the velocity, we will impose a no-slip boundary condition on all walls of the box. This will create boundary layers. Thus, when we will create the mesh we will need to refine our grid next to the borders to have well-defined boundary layers and gradients. For the temperature, we will have different boundary conditions. The vertical walls around the box, representing part of the Antarctica's ground, will have an adiabatic boundary condition: we will impose a zero flux through these walls. At the bottom of the box, we will simulate the geothermal flux. Thus, we will impose the derivative of the temperature along the z-axis. At the top of the box, the flux will be free but we will impose the temperature, to simulate the temperature gradient between thick and thin ice.

The gradient at the top of the simulation is represented by a sinus of amplitude  $\frac{\lambda L_x}{2}$  and of period  $2L_x$ . We use a sinus to accommodate the no flux conditions on the side walls. At the bottom of the simulation, it is the flux  $F$  that is imposed. Thus, with first dimensional variables (for clarity purposes we use them temporarily) we have:

$$T(x, y, H) = \frac{\lambda L_x}{2} \sin\left(\frac{\pi x}{L_x}\right) \text{ with } x \in \left[-\frac{L_x}{2}, \frac{L_x}{2}\right]. \quad (22)$$

$$\frac{\partial T}{\partial z} \Big|_{z=0} = \frac{-1}{k} F. \quad (23)$$

We can now use the dimensionless variables defined by equation (6) and the relation (7):

$$\bar{T}(\bar{x}, \bar{y}, \bar{H}) = \frac{\lambda k \bar{L}_x}{2F} \sin\left(\frac{\pi \bar{x}}{\bar{L}_x}\right) \text{ with } \bar{x} \in \left[-\frac{\bar{L}_x}{2}, \frac{\bar{L}_x}{2}\right]. \quad (24)$$

$$\frac{\partial \bar{T}}{\partial \bar{z}} \Big|_{\bar{z}=0} = -1. \quad (25)$$

Therefore, without the overlines and using the definitions of  $\Lambda$  and  $\Gamma$  from equations (20) and (21):

$$T(x, y, 1) = \frac{\Lambda \Gamma}{2} \sin\left(\frac{\pi x}{\Gamma}\right) \text{ with } x \in \left[-\frac{\Gamma}{2}, \frac{\Gamma}{2}\right]. \quad (26)$$

$$\frac{\partial T}{\partial z} \Big|_{z=0} = -1. \quad (27)$$

Then, for velocity, we will have at the walls (we continue to use dimensionless values without overlines here):

$$\mathbf{u}\left(-\frac{L_x}{2}, y, z\right) = \mathbf{u}\left(\frac{L_x}{2}, y, z\right) = \mathbf{u}\left(x, -\frac{L_y}{2}, z\right) = \mathbf{u}\left(x, \frac{L_y}{2}, z\right) = \mathbf{u}(x, y, 0) = \mathbf{u}(x, y, H) = 0. \quad (28)$$

And for the temperature at the side walls we will have:

$$\begin{cases} \frac{\partial T}{\partial x} \Big|_{x=-\frac{L_x}{2}} = \frac{\partial T}{\partial x} \Big|_{x=\frac{L_x}{2}} = 0 \\ \frac{\partial T}{\partial y} \Big|_{y=-\frac{L_y}{2}} = \frac{\partial T}{\partial y} \Big|_{y=\frac{L_y}{2}} = 0. \end{cases} \quad (29)$$

### 3.3 Initial condition

At the beginning of the simulation, there will be a transient state, with rapid variations. This state doesn't interest us and is computationally costly. Therefore we want to minimize it. For this purpose we will use as initial condition zero velocity and a uniform temperature everywhere, with small random variations in temperature to initiate the convection if the system has enough energy. Of course this initial state does not respect the boundary conditions and will consequently create a transient state, but it is still empirically the best initial condition in that regard.

### 3.4 Implementation in Nek5000

We will run our different simulations using the open source spectral element code Nek5000. For high enough Rayleigh, we will run the simulations over one diffusive time. We will obtain the data of the simulation in three different forms. First, Nek5000 will produce field files (with the extension .fld) that we will be able to visualize using the software visIt. Second Nek5000 will compute volume or surface averaged values and save them in a fort files, which we will analyze using Python routines. And finally we will place probes at fixed points in the domain to obtain the velocity, temperature and pressure at these points, which will be saved in text files that we will also analyze using Python.

We tried using the minimum computational resources for each of our simulations. The easiest simulations, at low Rayleigh numbers and weak rotation, were able to be calculated with 1596 spectral elements, distributed over 16 cores and with a spectral order of 6. These simulations lasted between a few hours and a week. For the more ambitious simulations, with high Rayleigh number and small Ekman number, the simulations were running with up to more than 9000 spectral elements, distributed over up to 256 cores regrouped on 8 nodes, and with a spectral order of 16.

We programmed our simulations to last over one diffusion time, enough to reach the stationary state for most of the simulations. However, the computation was interrupted by the PSMN, the supercomputer of the ENS on which we were running our simulations, after one week of calculation. In such very common cases, we restarted the simulations where they stopped only if they had not reached a clearly statistically steady state.

Finally, to have a good enough spatial resolution for our post-treatment of the results, we distributed 58779 probes across our domain to save the value of velocity, temperature and pressure at their position every 1000 time steps, corresponding roughly to between  $10^{-4}$  and  $10^{-3}$  of normalized time duration for the hardest simulations.

## 4 Pure Rayleigh-Bénard and Horizontal convection

The configuration and parameters of our interest to study the competition between Horizontal Convection and Rayleigh-Bénard convection motivated by subglacial lakes don't find really good fit in the literature, even though they are two well-studied phenomena. Indeed, most of the other simulations are done with periodic boundary conditions for the side walls, and often free-slip boundary conditions on top and bottom walls.

In this section we will first focus on pure Rayleigh-Bénard convection or pure horizontal convection, because by having a confined fluid, an aspect ratio of 4, rotation and at the same time imposing the flux and not the temperature, we observe the same tendencies as the previous works on Rayleigh-Bénard and Horizontal convection, but not a perfect match. Therefore, we cannot predict in advance the precise transitions that are important for our work. The purpose of these simulations will thus be to determine the effect of the confinement and rotation on the convection, and to determine the different regimes that we can observe so that we can choose the bests Rayleigh number for the study of the transitions in mixed RB and HC cases.

### 4.1 Without rotation

To isolate the effect of confinement alone, we will first consider RB and HC without rotation. Thus we have  $Ek = \infty$  and we fix the Prandtl number at  $Pr = 1$  as a first step for simplicity, as explained by appendix A. We run simulations with different Rayleigh numbers  $Ra$ .

#### 4.1.1 Rayleigh-Bénard convection

In this section we study pure RB, i.e.  $\Lambda = 0$ . To study the regimes of convection, we will use classical output dimensionless numbers. The first one is the Nusselt number, that evaluates the importance of the convection by comparing the heat transfer due to the convection to the one due to thermal diffusion. This Nusselt number is obtained by calculating the ratio between the heat flux through the box and the theoretical one if there were only diffusion.  $Nu = \frac{Q_{measured}}{Q_{diffusion}}$ .

In our case, we impose the heat flux  $F$ . Therefore, as  $Q_{diffusion} = -\Delta T_{vertical} \kappa H$ , we have (with dimensional variables):

$$Nu_{RB} = \frac{F}{\Delta T_{vertical} \kappa H}. \quad (30)$$

Using the dimensionless temperature defined in equation (6) with the reference temperature defined by equation 7, we obtain:

$$Nu_{RB} = \frac{1}{T_{bottom} - T_{top}}. \quad (31)$$

As done by [1], we take the averaged value for the bottom temperature, and the minimum value at the top of the domain to accomodate the mixed cases, where we have both RB and HC. Thus the Nusselt number becomes finally:

$$Nu_{RB} = \frac{1}{\langle T_{bottom} \rangle_{xy} - T_{min}}. \quad (32)$$

This dimensionless number characterizes the flow regime in buoyancy-driven convection such as the convection we will study here. Since we force our Rayleigh-Bénard convection with a heat flux, we will use the same the definition of the Rayleigh number as in [1],

$$Ra_F = \frac{g\alpha FH^4}{k\nu\kappa}. \quad (33)$$

But, as in the literature the Rayleigh number based on a temperature difference  $Ra_T$  is more used, we will use it in our results, by rescaling our Rayleigh number by the Nusselt number:

$$Ra_T = \frac{Ra_F}{Nu_{RB}}. \quad (34)$$

This relation is more detailed in the appendix B.1.

#### 4.1.1.1 Nusselt scaling and temperature profile

The Nusselt number is a very studied parameter, and in particular its scaling with the Rayleigh number. Indeed, the apparition and strengthening of the convection (due to increase of  $Ra_F$ ) typically increases the heat transfer through the box. It is an interesting parameter for us because the heat transfer inside the box will not only be affected by  $Ra$ , but also by our other controlling parameters, that is to say the confinement and the rotation, two important secondary parameters of our simulations. We will show that they tend to reduce the heat transfer by diminishing convection. One of the most interesting aspect for us is that the confinement and rotation will not affect the Nusselt for all Rayleigh numbers: for a high Rayleigh number, the convection will be strong enough not to be affected by the rotation. In fact, the difference in Nusselt between rotating and non-rotating RB convection is often used to define the different regimes of rotating RB convection (rotation dominated, rotation affected and rotation unaffected as defined by [4]). Therefore, we will start by characterizing the evolution of the Nusselt number with the Rayleigh number without rotation; then we will vary  $Ek$  to study the effect of rotation.

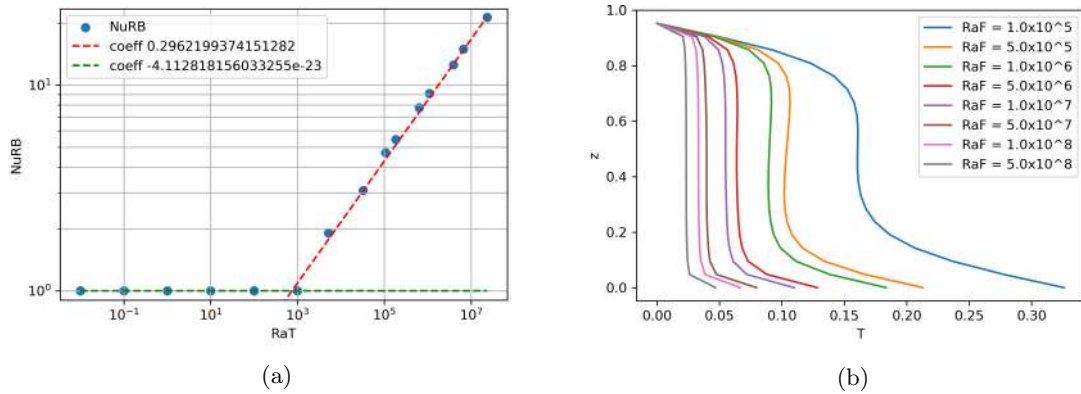


Figure 2: (a) Evolution of the Nusselt number  $Nu_{RB}$  with the Rayleigh number based on the top to bottom temperature difference  $Ra_T$  (b) Evolution of the temperature profile with the Rayleigh number  $Ra_F$ .

Before discussing our results we would like to make a note about the role of confinement on Rayleigh-Bénard convection. According to [10], confinement can offset the beginning of convection.

Indeed, for an infinite horizontal domain, the threshold at which the instability becomes strong enough and goes from a diffusive regime to a convective regime is at  $Ra_T = 1708$ , as explained by [2]. But the presence of walls with no-slip boundary conditions creates a viscous constrain that also has to be overcome to start the convection. [12] gives a relation between the aspect ratio and the critical Rayleigh number.

In our case, this critical Rayleigh number would be around the unity, which is below the critical Rayleigh number in an infinite domain. Confinement should therefore not be a limiting factor for the onset of RB convection. And as we can see on figure 2a, the threshold of convection is where it would be for an infinite domain (a precise threshold would require more simulations, but is not necessary for our study).

Figure 2a shows the evolution of  $Nu_{RB}$  with  $Ra_T$ , defined by equation (34). A commonly admitted scaling for our range of Rayleigh number, as can be found in [3], is  $Nu \propto Ra_T^{\frac{2}{7}}$  with  $\frac{2}{7} \approx 0.28$ . We can see on figure 2a that we have a good fit of our simulations with the theoretical scaling.

We can complement this evolution of the Nusselt number by looking at the temperature profile on figure 2b. Indeed, in Rayleigh-Bénard convection, the heat transfer happens at the top and bottom thermal boundary layers, whereas the bulk is well-mixed by the convection. As we increase the Rayleigh number, and thus the convection and the heat transfer associated, we expect the thermal boundary layers at the top and bottom of the domain to get thinner and the bulk to get more homogeneous in term of temperature. And this is precisely what we can observe.

Looking at figure 2b we can also notice the effect of imposing the heat flux and not the boundary temperature at the bottom of the domain: the top of the domain stays at  $T = 0$  but the bottom gets colder as the heat transfer becomes more efficient: to maintain the same heat flux, the temperature difference becomes smaller. This justifies our definition of the Nusselt number.

#### 4.1.1.2 Reynolds number

Another parameter that we can look at is the Reynolds number of our flow. In our dimensionless problem, the Reynolds number corresponds simply to the root mean square (RMS) velocity in our domain,

$$Re = \sqrt{\iiint_V \mathbf{u}^2 dV} \quad (35)$$

as used by [1]. On figure 3 we can see the offset of convection for the same value of Rayleigh number around  $Ra_T \approx 10^3$ , corresponding to the value already predicted. As we will see later, we also have an asymptotic scaling of the Reynolds number with the Rayleigh number:  $Re \propto Ra_T^{0.5}$ , corresponding to what can be found in the literature.

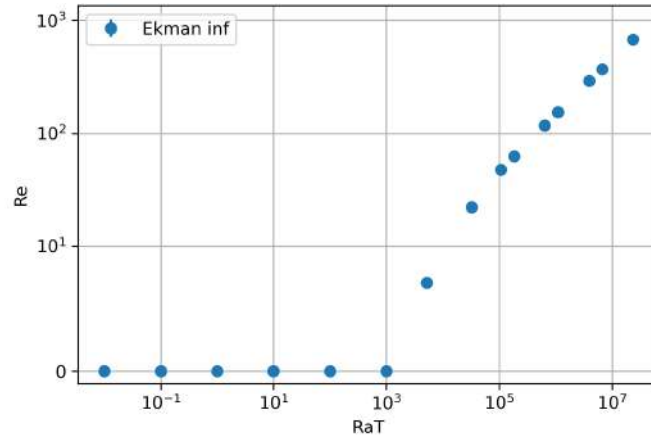


Figure 3: Evolution of the Reynolds number with the Rayleigh number for pure Rayleigh-Bénard convection without rotation. On this graph and all the following ones that are not temperature profiles, the vertical bars correspond to the temporal standard deviation of the variable in the simulation.

#### 4.1.1.3 Visualization

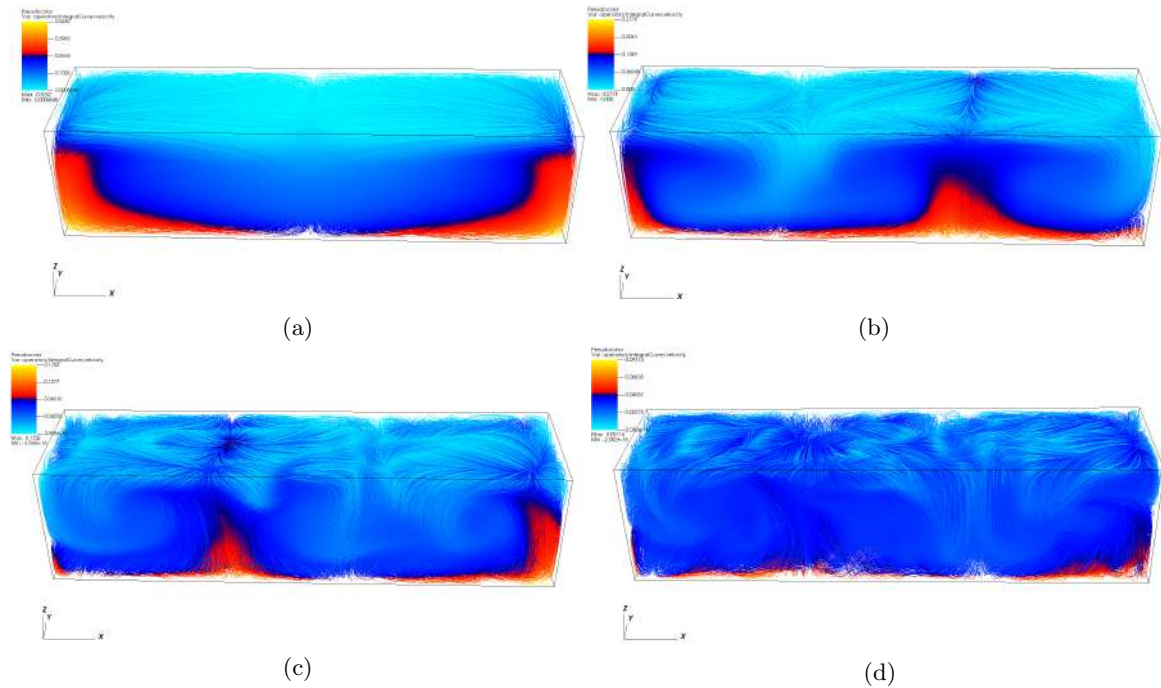


Figure 4: Snapshot of the streamlines of pure Rayleigh-Bénard convection simulations without rotation (i.e.  $Ek = \infty$ ), colored by the temperature, taken at the end of the simulations. (a)  $Ra_F = 10^5$  (b)  $Ra_F = 10^6$  (c)  $Ra_F = 10^7$  (d)  $Ra_F = 10^8$ .

A Rayleigh-Bénard cell consists of hot fluid going up on one side of the cell, getting colder at the top and then going down on the other side of the cell. In a perfect case, that is to say an unbiased flow (for example not a tilted box), there are no preferred direction, the only condition being that two consecutive cells must turn in opposite direction. The number of cells that we will have is dependent on the shape of the box. In our case, as we can see on figure 4, for  $Ra_F = 10^5$  there are two cells, for  $10^6 \leq Ra_F \leq 10^8$ , we have three cells for our shape of the domain.

On figure 4 we can clearly see the RB convection cells and all the phenomena described previously. As we increase the Rayleigh number, we can see the cold and hot fluid being confined to two thin layer at respectively the top and bottom of the domain, and the bulk getting more homogeneous. As we increase the Rayleigh, we also have the flow getting more turbulent and the cells getting less well-defined.

#### 4.1.2 Horizontal convection

Now that we have seen Rayleigh-Bénard convection, we can look at Horizontal Convection also without rotation. We will use similar parameters to study the evolution of Horizontal Convection, but we will need to adapt them. Indeed, their definitions based on Rayleigh-Bénard convection are not suited for the Horizontal Convection case.

First there is the input Rayleigh number. The one we impose in our simulations is  $Ra_F$  (defined by equation (33)), based on the flux imposed at the bottom of the domain. Since this flux is not the driving force of Horizontal Convection, we have to define an other Rayleigh number, associated with Horizontal Convection, so that we can compare our results to the literature:

$$Ra_L = \frac{g\alpha\lambda L^4}{\nu\kappa} \quad (36)$$

with  $\lambda$  the temperature gradient. It is link to the Rayleigh number we impose in our simulations by:  $Ra_L = \Gamma^4 \Lambda Ra_F$ , this relationship is detailed in the appendix B.1. Note that we obviously turn off geothermal heating when studying pure HC, i.e. by replacing the bottom BC with  $\frac{dT}{dz} = 0$ .

The Nusselt number is also different because HC drives first and foremost horizontal convective flows, not vertical ones. We will take the expression used by [1]:

$$Nu_{HC} = \frac{\langle T(z=1)\partial_z T(z=1) - T(z=0)\partial_z T(z=0) \rangle_{xy}}{\langle T_{diff}(z=1)\partial_z T_{diff}(z=1) - T_{diff}(z=0)\partial_z T_{diff}(z=0) \rangle_{xy}}. \quad (37)$$

The denominator, whose calculation is detailed in the appendix B.3, has different values whether there is a non zero flux at the bottom of the box or not:

$$\begin{cases} 1 + \frac{\Lambda^2 \Gamma \pi}{8} \tanh\left(\frac{\pi}{\Gamma}\right) & \text{if } \bar{F} = 1 \\ \frac{\Lambda^2 \Gamma \pi}{8} \tanh\left(\frac{\pi}{\Gamma}\right) & \text{if } \bar{F} = 0. \end{cases}$$

#### 4.1.2.1 Nusselt scaling

The Nusselt number will also be a great tool for the study of Horizontal Convection. Indeed, depending on the rotation and the confinement we will not have the same evolution of the Nusselt number with the Rayleigh number and it will therefore allow us to define different regimes for the Horizontal Convection (Extreme rotation, strong rotation, medium and weak rotation as defined by [9]). As for the RB convection, by sweeping in Rayleigh number we will go through those different regimes for any fixed rotation rate ( $Ek$ ).

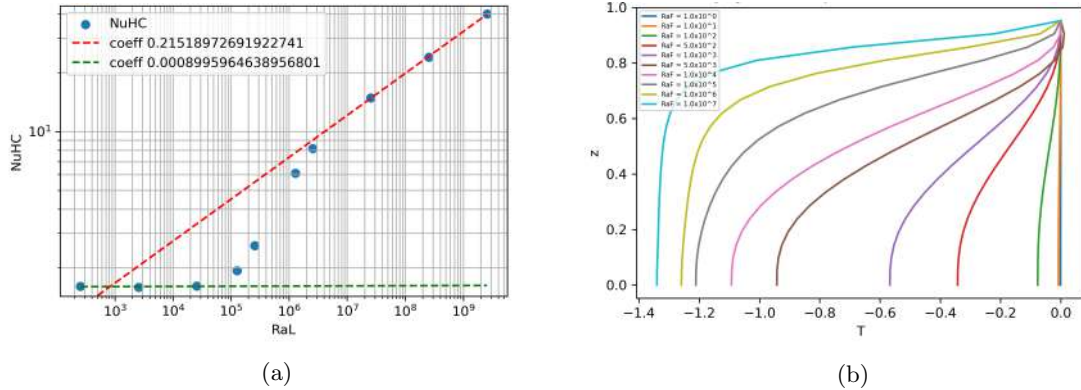


Figure 5: Evolution of the Nusselt number  $Nu_{HC}$  (a) and the temperature profiles (b) with the Rayleigh number  $Ra_L$  for the Horizontal Convection without rotation ( $Ek = \infty$ ).

The first element we have to take into consideration is that, contrary to the RB convection, there is always convection. The consequence is that the Nusselt number will never converge to 1 as we decrease the Rayleigh number. Instead, below a certain threshold, it reaches a plateau, which is higher than one, as we can observe on figure 5a. But, according to [12], these threshold and onset depend on the aspect ratio. In the following work, the aspect ratio is fixed, so the thresholds and onsets may vary only because of the rotation, but varying the aspect ratio could be a natural follow-up to this study and thus this effect should be kept in mind.

On figure 5a, we can see the different regimes of our flow when we increase the Rayleigh number. First, we have a Nusselt number which is independent of the Rayleigh number up to  $Ra_L \approx 10^5$  with the value  $Nu_{HC} \approx 1.6$ . Then, for  $Ra_L \geq 10^7$ , we reach a high Ra regime, where we have the classical scaling for Horizontal convection  $Nu_{HC} \propto Ra^{\frac{1}{5}}$  consistent with [12], with  $\frac{1}{5} = 0.2 \approx 0.22$ . We conclude that we have a good match between the scaling in the literature and the one we have obtained. On figure 5b we can see the creation of a cold layer at the bottom of the domain, as we will see on figure 7. We will describe it more thoroughly at that time.

#### 4.1.2.2 Reynolds number

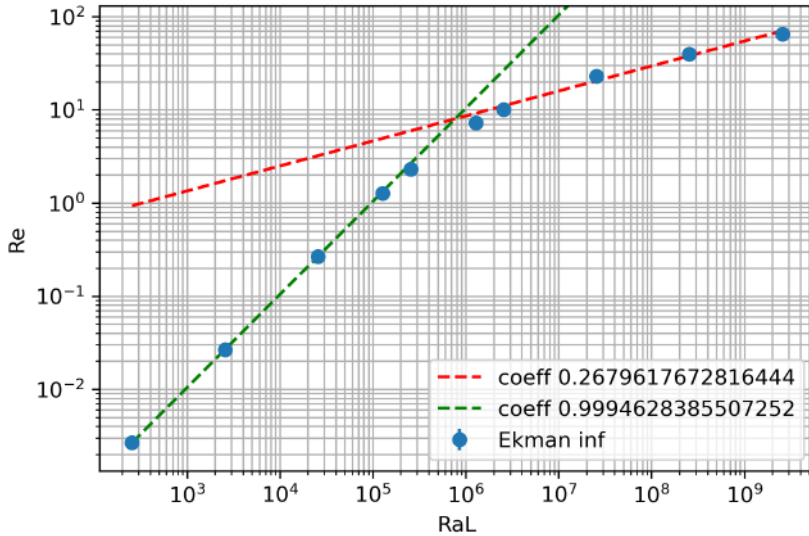


Figure 6: Evolution of the Reynolds number with the Rayleigh number for Horizontal Convection without rotation.

The Reynolds number showed on figure 6 confirms the two regimes that we have already identified with the Nusselt number, with the same  $Ra_L = 10^6$  for the transition. For  $Ra_L \leq 10^6$  we have a very small Reynolds, scaling as  $Re \propto Ra_L$ , corresponding to the diffusive regime where thermal diffusion dominates heat transfer and the flow is linearly driven by buoyancy anomaly along the top boundary and viscosity. Then, for  $Re \geq 10$  and  $Ra_L \geq 10^6$  we enter a second regime, where  $Re \propto Ra_L^{0.27}$ . This is the convection regime, corresponding to the scaling  $Nu_{HC} \propto Ra_L^{\frac{1}{5}}$  on figure 5a.

#### 4.1.2.3 Visualization

Finally, we can look at the structure of the flow, by calculating the streamlines, and the distribution of temperature.

For  $Ra_L \leq 10^6$  ( $Ra_F \leq 5 \cdot 10^3$ ), we have the viscous regime: the thermal diffusion dominates the heat transfer and the circulation of the fluid is a slow roll over the entire domain, going from hot to cold on the top of the box, and from cold to hot at the bottom. This is what we can see on figure 7a. On figure 7b we are still in the viscous regime, but as we are getting very close to the transition to inertial regime, as  $Ra_F = 10^3$ , the temperature distribution starts to be influenced by the flow. Therefore we can see the beginning of the formation of the cold layer at the bottom of the box, that is apparent on figure 5b.

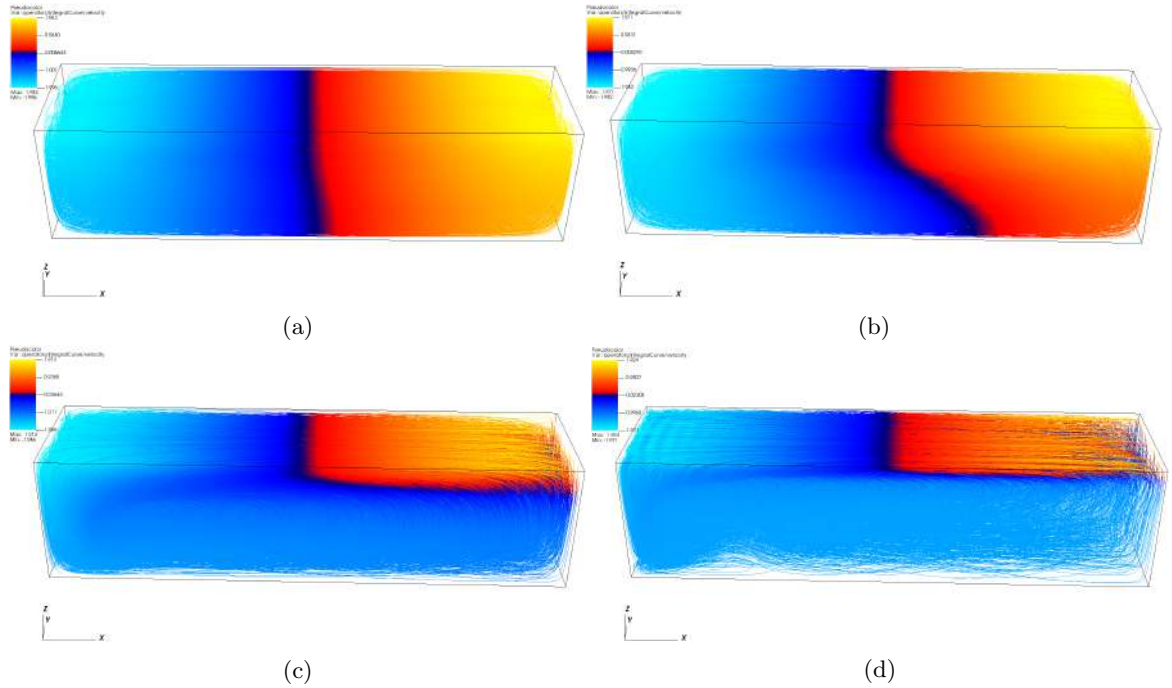


Figure 7: Snapshot of the streamlines of pure Horizontal convection simulations without rotation (i.e.  $Ek = \infty$ ), colored by the temperature, taken at the end of the simulations. (a)  $Ra_F = 10^2$  (b)  $Ra_F = 10^3$  (c)  $Ra_F = 10^5$  (d)  $Ra_F = 10^7$ .

On figures 7c and 7d we are in the inertial regime and we can recognize the typical circulation and temperature distribution of the Horizontal Convection. At the top of the domain, we have a thin layer, that gets thinner as we increase  $Ra_L$ , where the heat transfer is convective and most intense. In this thin layer, the fluid moves quickly from the hot wall where  $x \geq 0$ , to the cold wall where  $x \leq 0$ . There, after exchanging its heat, it is blocked by the wall and thus has to plunge to the bottom of the box in a cold plume. There the cold fluid, forming a stable cold layer that can be easily identified on figure 5b and that grows with the Rayleigh number, slowly goes back up to the top right of the domain, to be heated again.

To complement these observations and add an important aspect of Horizontal Convection to our study, we have to look at the horizontal velocity as well. Indeed, as explained by [7], the cold layer at the bottom of the box gets more and more stratified as we increase  $Ra_L$  and it becomes difficult for the plume to get through it, to the point where the return flow, instead of going through this layer, is condensed in an intrusion between the cold stratified layer and the hot convective layer at the top of the box. And it is this profile that we observe for the highest  $Ra_L$  on figure 8b compared to figure 8a: an important part of the return flow is in an intrusion between  $z = 0.6$  and  $z = 0.8$ . The rest of it is due to the plume that is blocked by the bottom wall of our box and thus gets to the right of our box. It can be noticed by the presence of the white spot between to red spots near the lower left corner of the box on figure 8b: there is a weak velocity between to jets.

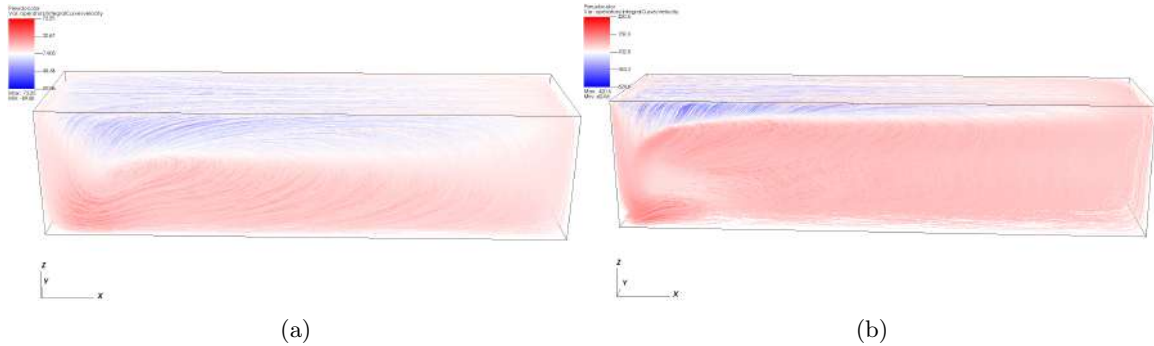


Figure 8: Snapshot of the streamlines of pure Horizontal convection simulations without rotation (i.e.  $Ek = \infty$ ), colored by the velocity along the x-axis, taken at the end of the simulations. (a)  $Ra_F = 10^5$  (b)  $Ra_F = 10^7$ .

## 4.2 With rotation

Now that we have studied the behaviour of our fluid for pure Rayleigh-Bénard convection and pure Horizontal Convection without the effect of rotation, we can add this phenomenon and explore its effects. It will allow us to determine the best parameters (Rayleigh number and Ekman number) for the different transition that we will later make. The effect of rotation on RB and HC have also previously been studied, but, as said before, never for the configuration of our interest. Thus, here we run our own simulations of rotating pure RB or HC, which we will interpret in light of previous published works.

### 4.2.1 Rayleigh-Bénard convection

#### 4.2.1.1 Nusselt number

The Nusselt number is one of the main criteria used in the literature to distinguish between the different regimes associated with rotation. Indeed, [4], compares the Nusselt number under rotation to the one without rotation for the Rayleigh-Bénard convection to determine whether the flow is dominated, affected or unaffected by rotation. If the Nusselt number is lower than expected, it typically means that rotation inhibits the convection and we can say that the flow is dominated by rotation. That being said, the Nusselt number can also be higher with rotation than without. This overshoot is due to the Ekman pumping, and is the criterion to say that the flow is affected (but not dominated) by rotation. Finally, if there is no difference between the two Nusselt numbers, then we can say that the flow is unaffected by the rotation. The same principle applies to Horizontal Convection.

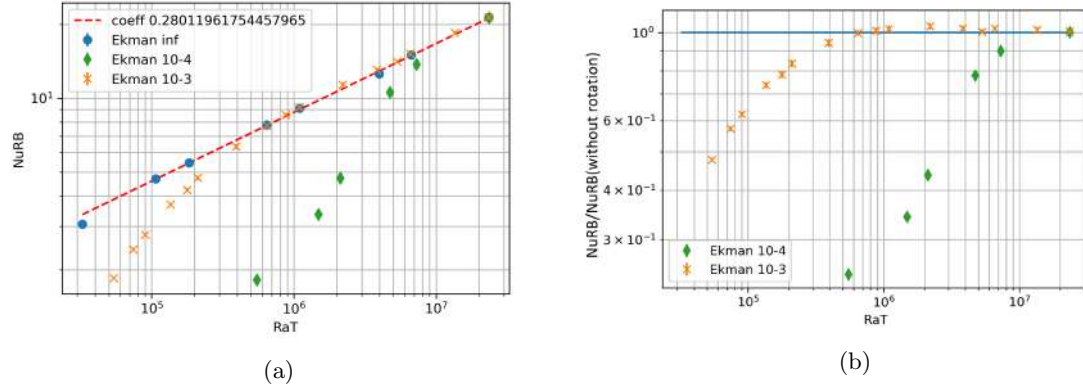


Figure 9: Evolution of the Nusselt numbers  $Nu_{RB}$  (a) and the Nusselt number normalized by the Nusselt number without rotation (b) with the Rayleigh number ( $Ra_T$ ), colored by the Ekman number ( $Ek$ ) for the Rayleigh-Bénard convection.

As we can see on figure 9a, we have a great convergence of the Nusselt numbers under rotation toward the Nusselt numbers without rotation as we increase the Rayleigh number, as predicted by [5]. Moreover we can observe that we have the correct relationship between the Nusselt as we diminish the Ekman number, that is to say, as we increase the rotation:  
 $Nu_{RB}(Ek = 10^{-4}) < Nu_{RB}(Ek = 10^{-3}) < Nu_{RB}(Ek = \infty)$ .

To more thoroughly compare the Nusselt numbers, we can also rescale each Nusselt number by the Nusselt number obtained without rotation ( $Ek = \infty$ ). That way, we obtain immediately the different regimes described by [4]. On figure 9b, we can observe that for  $Ra_T < 6 \cdot 10^5$  and  $Ek = 10^{-3}$ , the Nusselt number is much smaller than the non-rotating one, thus showing that we are in a rotation dominated regime. The same thing can be said for  $Ra_T < 10^7$  and  $Ek = 10^{-4}$ .

These values are coherent with the results of [4] and [5], although we do not have a perfect match for two reasons. First we do not necessarily use the same container geometry for our study, a cylinder being used often for rotating RB convection. This difference could affect the scaling, the question being addressed by [11]. Secondly, and more importantly, we simulate confined rotating Rayleigh-Bénard convection. And a very important consequence is the creation of wall modes.

Indeed, even below the predicted critical Rayleigh number  $Ra_c$ , as defined by [2], where there should be no convection possible, the presence of the walls allow a form of convection, close to them, as we can see on figure 9a. Therefore the heat flux, and the Nusselt number, are higher than they should. This effect can not be seen for simulations made with periodic boundary conditions.

#### 4.2.1.2 Temperature profiles

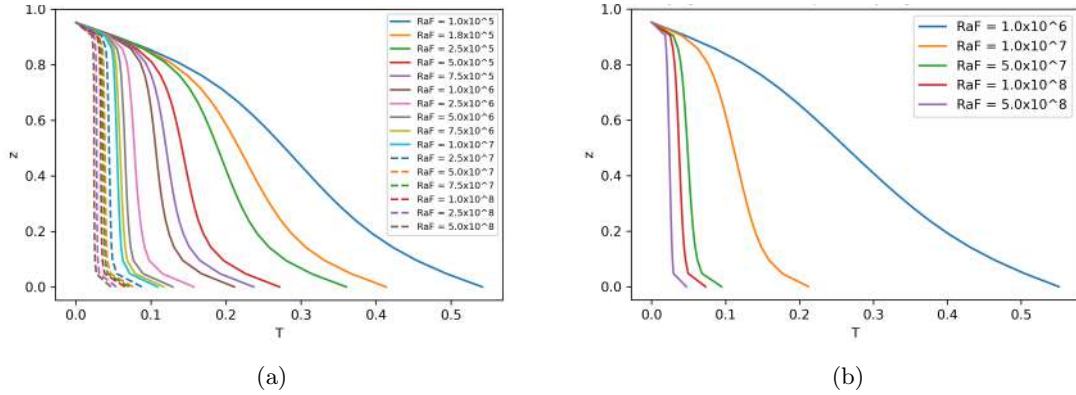


Figure 10: Evolution of the temperature profile with the Rayleigh number  $Ra_F$  for rotating Rayleigh-Bénard convection. The dashed lines are here to differentiate two lines with the same color. (a)  $Ek = 10^{-3}$  (b)  $Ek = 10^{-4}$ .

As we have explained and shown previously, as we increase the Rayleigh number, the bottom temperature diminishes, the temperature gradient between the top and bottom walls gets concentrated in two thinner boundary layers at the top and bottom of the domain, and in between the bulk gets more mixed, and thus thermally homogeneous. The rotation delays this evolution. We obtain for Rayleigh number high enough the same temperature profiles, the regime that we call rotation unaffected. But for lower  $Ra_F$  the rotation inhibits the mix of the bulk. To better see this effect, we can compare the temperature profile of simulations at an identical  $Ra_F = 10^6$  but for different Ekman numbers.

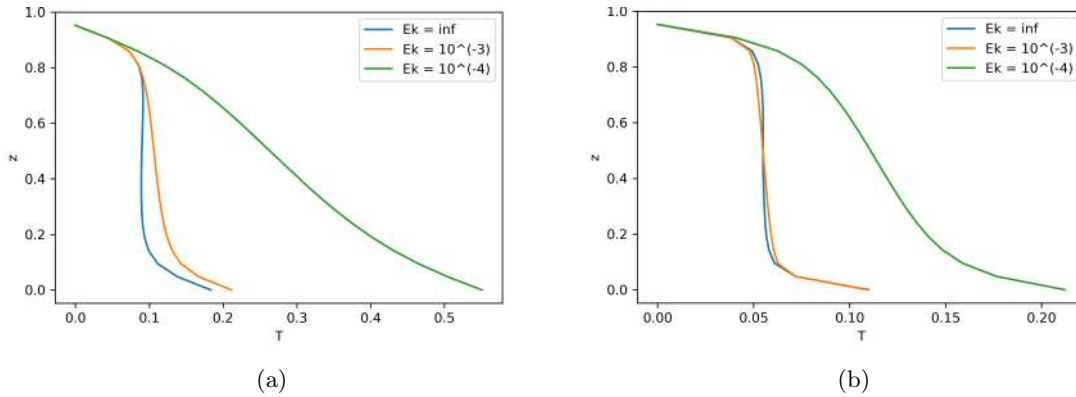


Figure 11: Comparison of the temperature profiles for different Ekman number ( $Ek = \infty, Ek = 10^{-3}, Ek = 10^{-4}$ ). (a)  $Ra_F = 10^6$  (b)  $Ra_F = 10^7$ .

As we can see on figure 11, as we diminish  $Ek$ , and thus increase the rotation, we augment the gradient of temperature in the bulk and thus the mean temperature. However, it is also interesting to see that the thermal boundary layers are identical in all three cases, as they are on top of each

other at the top of the domain. Since at  $Ra_F = 10^6$  we are reaching the end of the rotation-affected domain for  $Ek = 10^{-3}$ , we can see that its temperature profile is not very different from the one without rotation. Indeed, we can see on figure 11b that if we do the same thing for  $Ra_F = 10^7$ , the temperature profiles are identical for  $Ek = \infty$  and  $Ek = 10^{-3}$ .

#### 4.2.1.3 Reynolds numbers

As in section 4.1.2.2 we now turn our attention to the Reynolds number for pure RB convection with rotation, as it provides an interesting dynamical information. Moreover, we will decompose this Reynolds number into an horizontal Reynolds number, based on solely the horizontal component of the velocity and a barotropic Reynolds number. Indeed, we expect rotation to diminish the overall Reynolds number by inhibiting convection, but at the same time to increase the horizontal movement, at least respectively to the global Reynolds number, and even more importantly increase the barotropic Reynolds number, a dimensionless number corresponding to the velocity created by the rotation due to the Coriolis force.

The horizontal Reynolds is defined by the average of the horizontal component of the velocity:

$$Re_h = \sqrt{\frac{1}{V} \iiint_V (u^2 + v^2) dV}. \quad (38)$$

The barotropic Reynolds number is also defined with the horizontal component of the velocity but focuses on the depth-invariant component, i.e. the rotation created by the Coriolis force:

$$Re_b = \sqrt{\frac{1}{V} \iint_{xy} ((\int_z u dz)^2 + (\int_z v dz)^2) dx dy}. \quad (39)$$

With this definition, the horizontal velocity is compensated by any the return flow that occurs on the vertical axis.

We can observe the same tendency as for the Nusselt number in figure 9a: the Reynolds number with rotation joins the curve of non-rotating RB convection as we increase the Rayleigh number. But one interesting observation is that they join it much more later than the Nusselt number does, around  $Ra_T = 10^7$  for  $Ek = 10^{-3}$ . Indeed, this is here one of the difficult aspect of this study is that two simulations might have the same properties for transmitting heat, but not the same flow organization and structure. And this is illustrated by the Reynolds number amongst other. Note also that two simulations with the same Reynolds number may similarly have different Nusselt numbers as discussed in [1].

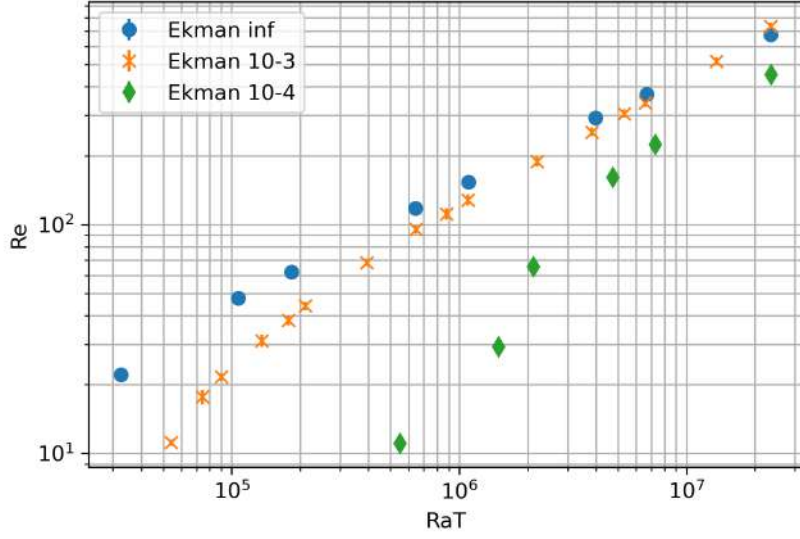


Figure 12: Evolution of the Reynolds number  $Re$  with the Rayleigh number  $Ra_T$ , colored by the Ekman number  $Ek$  for rotating Rayleigh-Bénard convection.

To further illustrate this aspect we can more closely look at this Reynolds number, by only taking the horizontal component of the velocity and comparing it to the barotropic component. If the Horizontal Reynolds number, figure 13b closely resembles the total Reynolds number, it is not the case for the barotropic Reynolds number, figure 13a. First of all, the barotropic Reynolds number for  $Ek = 10^{-3}$  and  $Ek = \infty$  are superimposed. Since the total Reynolds number is higher for the non-rotating simulations, it means that rotation has an impact on the circulation of the fluid. It is more complicated to interpret the curve for  $Ek = 10^{-4}$  since in all cases the Reynolds is smaller. To help the comparison, we can rescale those horizontal and barotropic Reynolds number by the total Reynolds number.

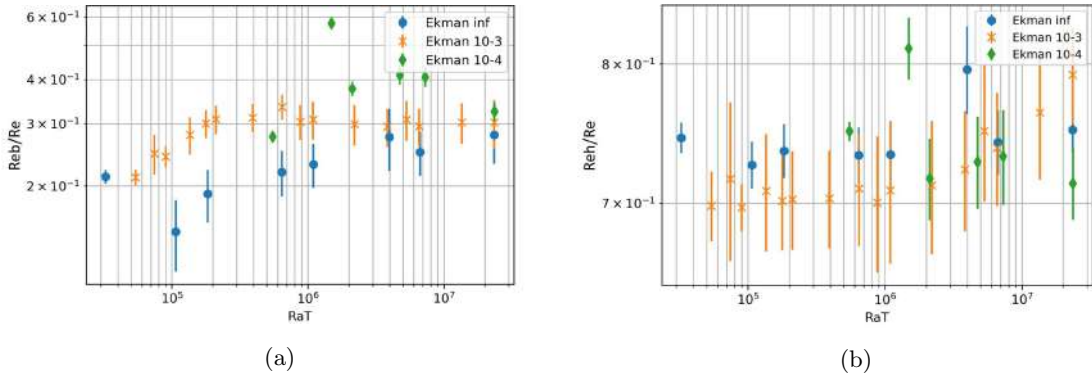


Figure 13: Evolution of the barotropic Reynolds numbers  $Re_b$  (a) and of the horizontal Reynolds number  $Re_h$  (b) with the Rayleigh number  $Ra_T$ , colored by the Ekman number  $Ek$ , for rotating Rayleigh-Bénard convection.

On figure 13b, we can notice that, with few exception, we have higher rescaled horizontal Reynolds

for  $Ek = \infty$  than for the other Ekman number and it is the inverse for the rescaled barotropic Reynolds. Moreover, we can notice that for the relative importance of the barotropic velocity, between  $Ra_T = 5.10^4$  and  $Ra_T = 10^6$  there is a 10% difference between  $Ek = 10^{-3}$  and  $Ek = \infty$  and then a convergence, the same phenomenon being true for  $Ek = 10^{-4}$  between  $Ra_T = 10^6$  and  $Ra_T = 10^7$ . It can be interpreted by regimes for which the rotation has more influence on the flow, before regimes where the flow is unaffected by it. These numbers are coherent with the regimes determined with the Nusselt numbers. Finally, we can notice that, even though the barotropic velocity can increase, it always stays at low values, around 30%, compared to the horizontal velocity, that climbs up to almost 80%.

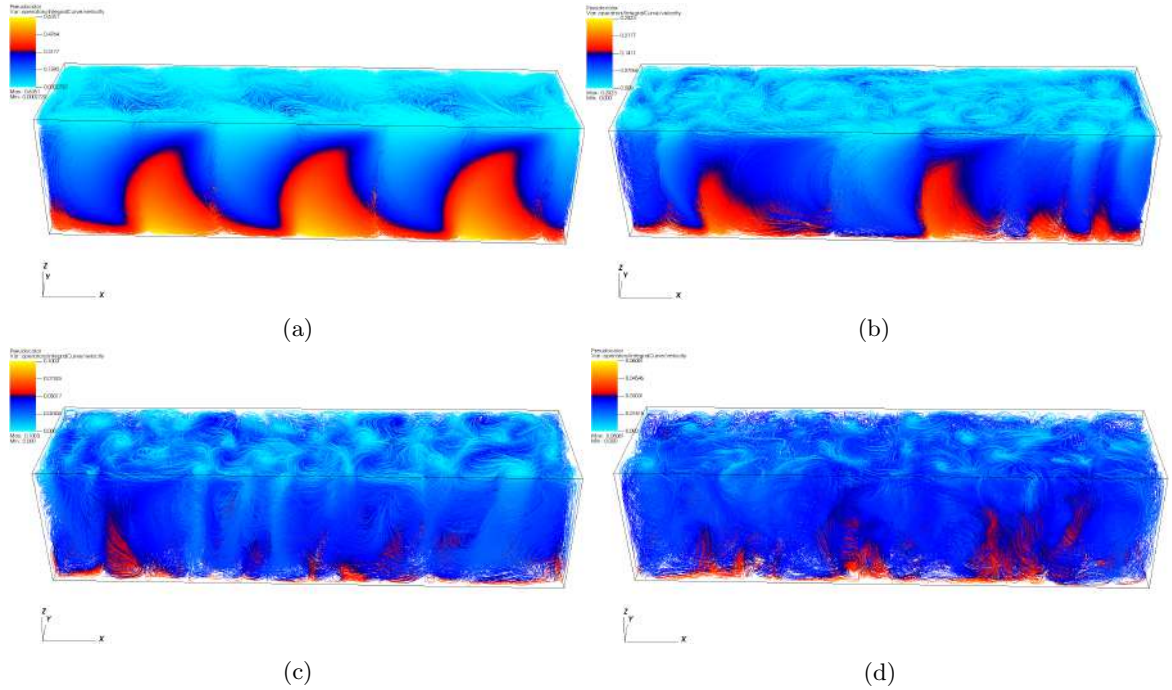


Figure 14: Snapshot of the streamlines of pure Rayleigh-Bénard convection simulations with rotation ( $Ek = 10^{-4}$ ), colored by the temperature, taken at the end of the simulations. (a)  $Ra_F = 10^6$  (b)  $Ra_F = 10^7$  (c)  $Ra_F = 10^8$  (d)  $Ra_F = 5.10^8$ .

On figure 14, we can see the evolution of the flow structure as we increase the Rayleigh number. On figure 14b, we have a Rayleigh number smaller than the critical Rayleigh number for  $Ek = 10^{-4}$ , but instead of having only a diffusion solution, we have convection in the form of wall modes as described by [6], as we will discuss it later. On figure 14c, we have a supercritical Rayleigh number, and therefore a fully developed rotating Rayleigh-Bénard convection, but, as we can see, there are still some non-negligible wall modes.

Moreover, we do not have the classical convective rolls, that can be seen on figure 4. Here, the convection takes the form of vertical swirls, either cold and forming at the top and going into the bulk, or hot and forming at the bottom and going into the bulk, which is evidence of rotation effects. Furthermore, we can notice that the bulk is getting more homogeneous as we increase the Rayleigh number, the temperature gradient being located closer and closer to the top and bottom of the box,

in thin layers, with the exceptions of swirls.

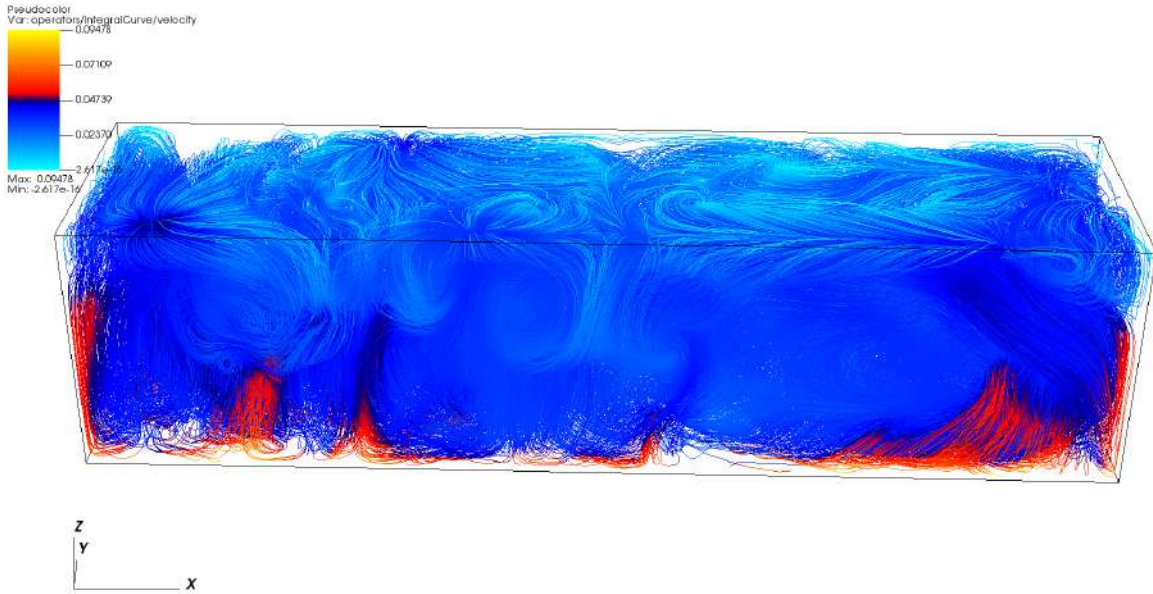


Figure 15: Snapshot of the streamlines of pure Rayleigh-Bénard convection simulations with rotation ( $Ek = 10^{-3}$ ), at  $Ra_F = 10^8$ , colored by the temperature, taken at the end of the simulation.

The study of the Reynolds number and the visualization of the streamlines are really relevant because simulations with identical Nusselt numbers  $Nu_{RB}$ , obtained for the same Rayleigh number  $Ra_F$  but with different Ekman number  $Ek$  can lead to totally different flows, as we can see on figure 15, which has the same Nusselt number for the same Rayleigh number as the RB convection without rotation, figure 4d but clearly a different flow structure.

#### 4.2.1.4 Wall modes

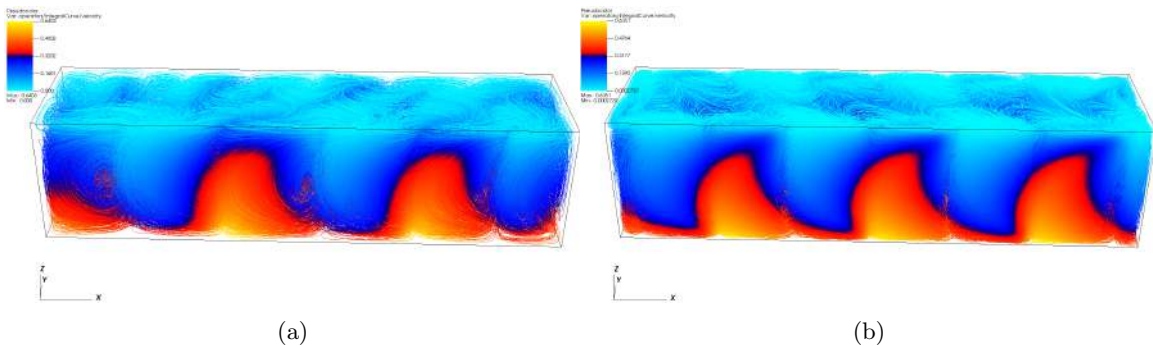


Figure 16: Snapshot of the streamlines of Wall modes for pure Rayleigh-Bénard convection simulations with rotation, colored by the temperature, taken at the end of the simulations. (a)  $Ek = 10^{-3}$ ,  $Ra_F = 10^5$  (b)  $Ek = 10^{-3}$ ,  $Ra_F = 10^6$ .

One interesting effect of the rotation in a confined domain, is that below the critical Rayleigh number, which is the threshold for convection, convection still takes place but in the form of Wall modes, as explained by [6]. Confined to the walls, with a thickness depending on the Ekman number, these convection cells rotates around the domain, contributing to the heat exchange. These walls modes, still present for supercritical Rayleigh number, have an influence on the Nusselt number among other thing and is the reason we do not have a perfect match with the literature, often calculated with periodic boundary conditions, and thus where there are no wall modes. This is why we have  $Nu_{RB} \geq 1$  for  $Ra \leq Ra_c$ .

#### 4.2.2 Horizontal Convection

Now that we have seen the effect of rotation on Rayleigh-Bénard convection, we can do the same investigation for Horizontal Convection. We expect the same effects, inhibition of the convection and of the heat transfer, modification of the structure of the flow ... but also effects specific to Horizontal convection, notably due to the fixed direction of currents near the top boundary.

##### 4.2.2.1 Nusselt number

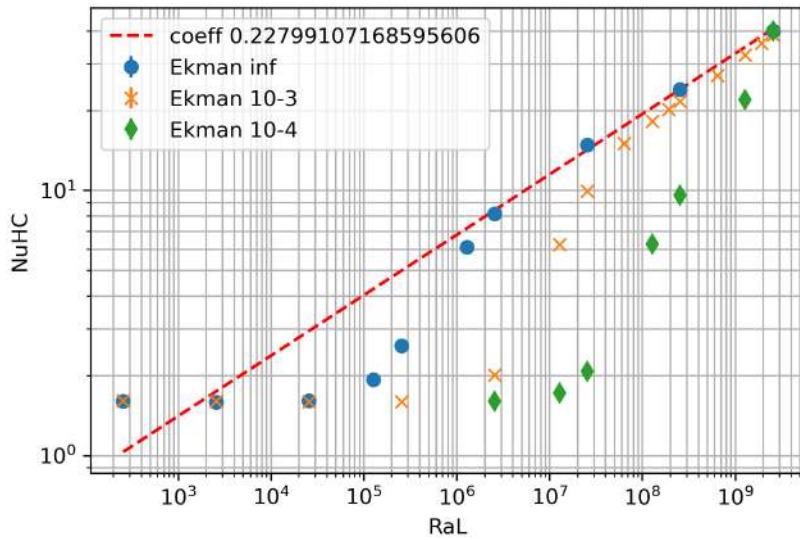


Figure 17: Evolution of the Nusselt number  $Nu_{HC}$  with the Rayleigh number  $Ra_L$ , colored by the Ekman number  $Ek$  for Horizontal Convection.

The first value we want to look at is the Nusselt number. On figure 17 we can notice three important features. Firstly, we can notice that the Nusselt number for all Ekman number converges to the same value for low Rayleigh numbers. It is interesting because it corresponds to a very viscous linear regime, where convection still affects the heat transfer, otherwise it would converge to one, but where the rotation does not impact it. The viscous force dominates the Coriolis force. Then, the Nusselt number also converge for high Rayleigh,  $Ra_L = 10^8$  for  $Ek = 10^{-3}$  and  $Ra_L = 2.5 \cdot 10^9$  for  $Ek = 10^{-4}$ . Once again we coherently reach the rotation unaffected regime later when the rotation

is stronger. Finally the transition between viscosity dominated flow to convection dominated flow is delayed by the rotation. The critical Rayleigh number required to quit the viscous regime is  $Ra_L = 5 \cdot 10^4$  for  $Ek = \infty$ ,  $Ra_L = 10^6$  for  $Ek = 10^{-3}$  and  $Ra_L = 2 \cdot 10^7$  for  $Ek = 10^{-4}$ .

#### 4.2.2.2 Temperature profiles

Finally we can look at the temperature profiles. On figure 18 we can see the establishment of the cold stable layer at the bottom of the domain and its growth as we increase the Rayleigh number. We can still notice on figure 18b that interestingly the bottom of the box is colder for  $Ra_F = 10^6$  than for  $Ra_F = 10^7$ . And on figure 19a we can see that for  $Ra_F = 10^6$  we indeed are very close to the rotation unaffected regime for  $Ek = 10^{-3}$  and clearly delayed for  $Ek = 10^{-4}$ . Then, on figure 19b we can see that all the simulations with rotation have reached the rotation unaffected regime, the temperature profiles for  $Ek = \infty$  and  $Ek = 10^{-4}$  being even superposed.

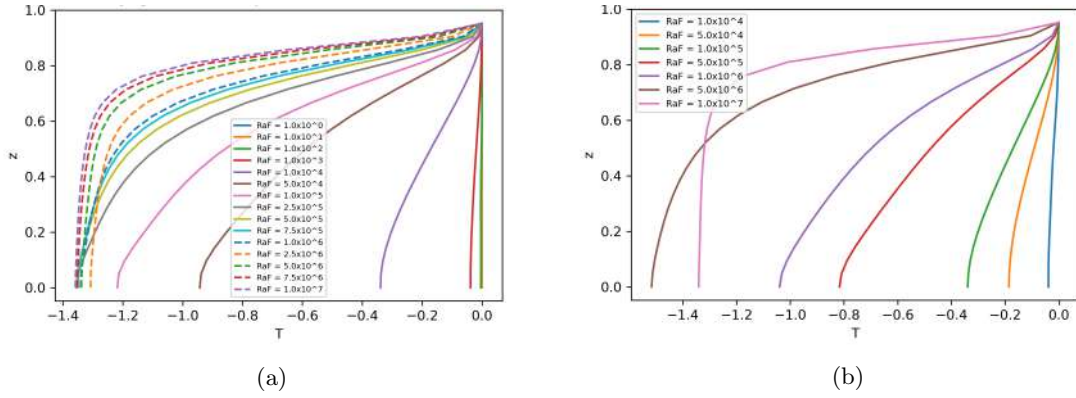


Figure 18: Evolution of the temperature profile with the Rayleigh number  $Ra_F$  and the Ekman number  $Ek$  for Horizontal Convection. The dashed lines are here to differentiate two lines with the same color. (a)  $Ek = 10^{-3}$  (b)  $Ek = 10^{-4}$ .

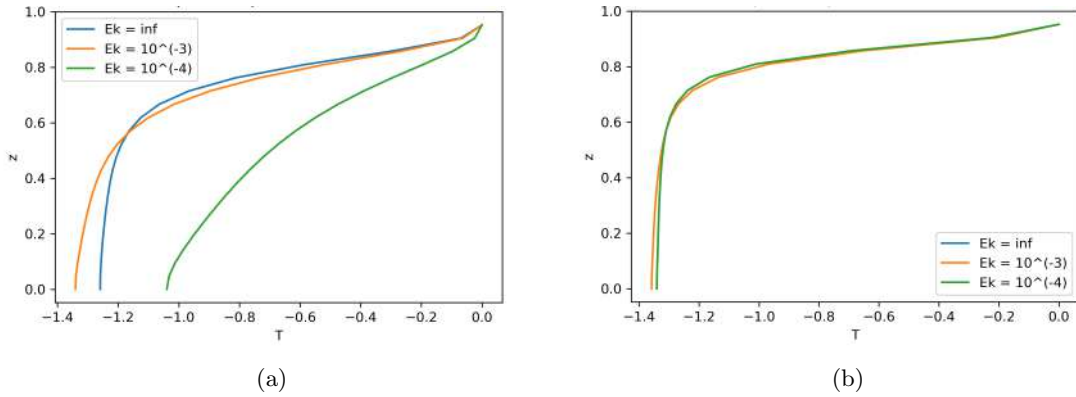


Figure 19: Comparison of the temperature profile for different Ekman number ( $Ek = \infty$ ,  $Ek = 10^{-3}$ ,  $Ek = 10^{-4}$ ) for Horizontal Convection. (a)  $Ra_F = 10^6$  (b)  $Ra_F = 10^7$ .

### 4.2.2.3 Reynolds numbers

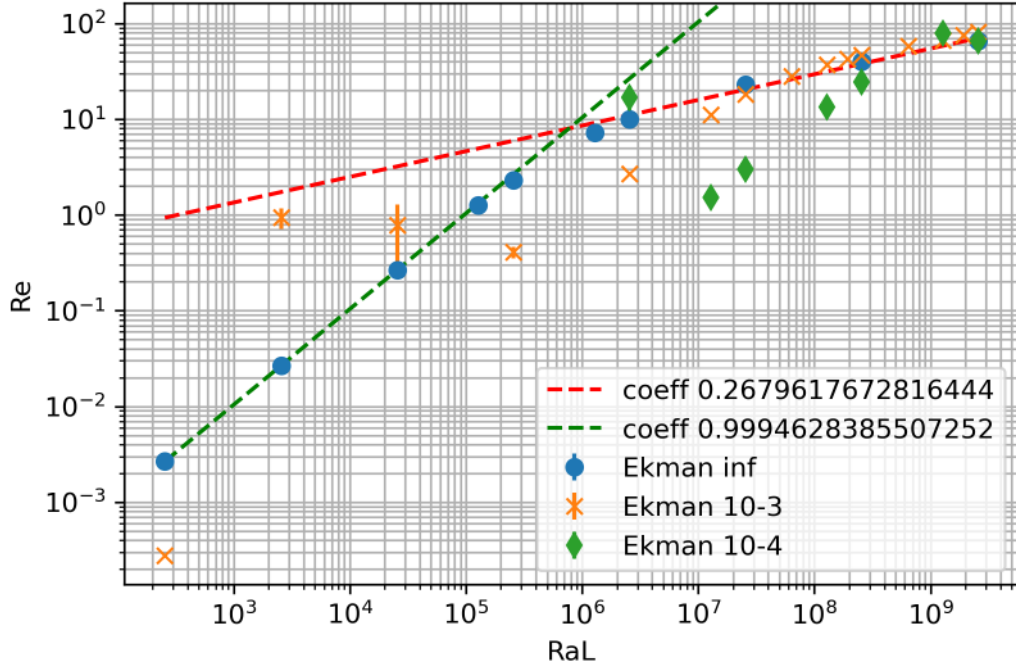


Figure 20: Evolution of the Reynolds number  $Re$  with the Rayleigh number  $Ra_L$ , colored by the Ekman number  $Ek$  for Horizontal Convection.

The behaviour of the Reynolds number adds an interesting aspect to the evolution of the fluid with the Rayleigh number. Without rotation, we can see on figure 20 a fast increase of the Reynolds number, with  $Re \propto Ra_L$ , up to  $Ra_L = 10^6$ , and then a second slope with the relationship  $Re \propto Ra_L^{0.27}$ . Interestingly, when we add rotation, at some point we have a decrease of the Reynolds number. At high Rayleigh number, we have a convergence. We lack simulations in the viscous domain to describe it precisely, but for  $Ek = 10^{-3}$ , we can observe a decrease from  $Ra_L \approx 10^3$  to  $Ra_L \approx 5 \cdot 10^5$ , which corresponds to the end of the viscosity-dominated regime as previously described.

For  $Ek = 10^{-4}$ , we also start with a decrease but with only one point, we can not interpret much, even though the rupture occurs at  $Ra_L = 10^7$ , which corresponds to the end of the viscous regime observed with the Nusselt number. Since we also have at very low Rayleigh number a very low Reynolds for  $Ek = 10^{-3}$ , and since there are no decrease without rotation, we can infer that it is an effect of rotation. It may be a rotation-dominated regime, that has the same heat transfer characteristics as the viscosity dominated regime, therefore invisible with the Nusselt number, but with a different Reynolds.

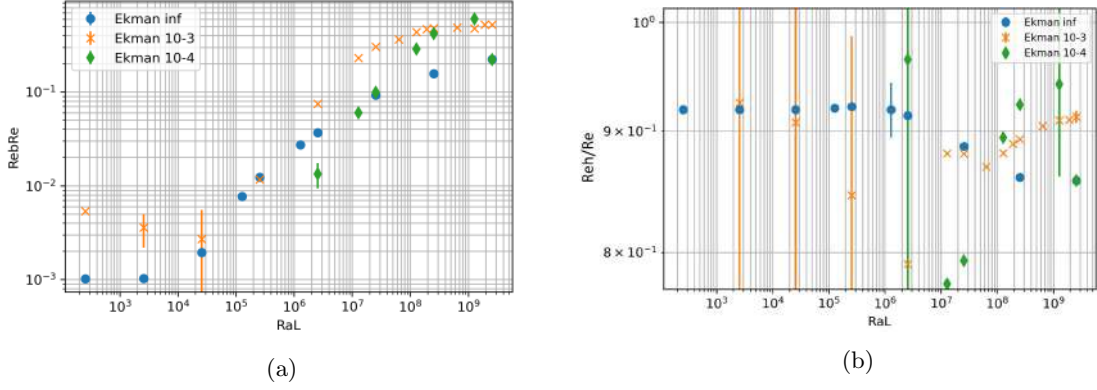


Figure 21: Evolution of the barotropic Reynolds numbers  $Re_b$  (a) and the horizontal Reynolds numbers  $Re_h$  (b) with the Rayleigh number  $Ra_L$ , colored by the Ekman number  $Ek$  for Horizontal Convection.

Looking at the horizontal Reynolds number and the barotropic Reynolds number we can refine our understanding of the evolution of the Reynolds number, figure 20. First, on figure 21b, without rotation, for low Rayleigh number the importance of the horizontal velocity is constant and very high:  $Re_{hor} \approx 90\%$ . It means that the movement is essentially horizontal, with a very weak upwelling and downwelling. Then, at  $Ra_L = 10^6$ , the relative horizontal Reynolds number starts diminishing, to stabilize at around  $Re_{hor} \approx 85\%$ . It corresponds to the end of the viscosity-dominated regime. The sinking of the cold fluid starts to intensify and to form a plume, while the overall velocity increases slowly, reducing the importance of the horizontal velocity.

When we add rotation, the behaviour changes. We know that Coriolis only affects horizontal velocity. Therefore, as we increase the Rayleigh number, we can see on figure 21b that the relative horizontal velocity decreases because the Coriolis inhibits it from increasing as fast as the vertical velocity, up to  $Ra_L = 5 \cdot 10^6$ . Then, as the flow is reaching a rotation independent regime, the relative horizontal Reynolds number increases to more than 90%, that is to say to a higher importance than without rotation for a reason that we will try to elucidate later. The horizontal Reynolds number for  $Ek = 10^{-4}$  follows the same evolution, amplified by a stronger rotation, and delayed to a transition around  $Ra_L = 10^7$ , coherent with the previous observations.

#### 4.2.2.4 Visualization

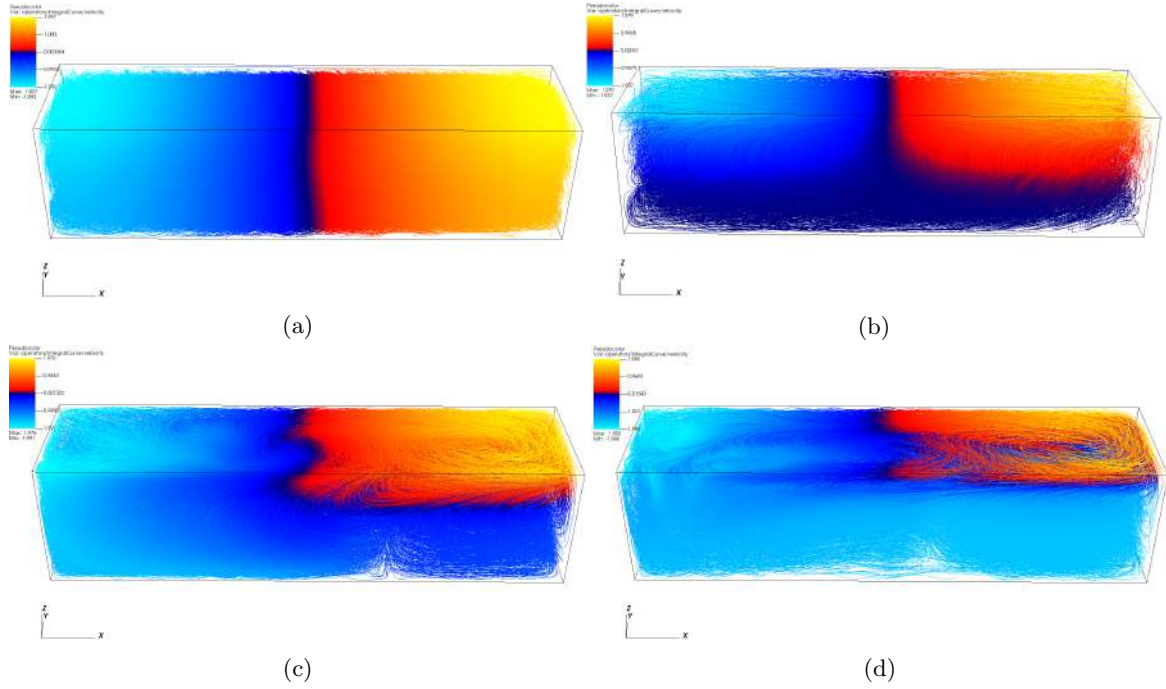


Figure 22: Snapshot of the streamlines of pure Horizontal convection simulations with rotation ( $10^{-4}$ ), colored by the temperature, taken at the end of the simulations. (a)  $Ra_F = 10^4$  (b)  $Ra_F = 10^5$  (c)  $Ra_F = 10^6$  (d)  $Ra_F = 10^7$ .

Looking at the flow structure on figure 22, we can see that rotation delays the transition to the convective regime. Indeed, if we compare 22a to 7b, which has a smaller Rayleigh number but is already more affected by the convection in term of temperature distribution, or 22b to 7c, both of them having the same Rayleigh number  $Ra_F$ , it is clear that the convection-dominated regime is delayed.

On figure 22d we can see that for a Rayleigh number high enough we can have approximately the same temperature distribution as the case without rotation, with a thin layer at the top where the heat exchanges take places, and a well-mixed cold layer at the bottom. Nevertheless, it does not mean that the flow structure is the same. As we can see on figures 22c and 22d, it is greatly influenced by vortices, easily noticeable on the top layer but also present from top to bottom, which is why the barotropic and horizontal Reynolds number from figure 21 is larger when the Ekman number is finite.

#### 4.2.2.5 Q criterion

Finally, we can consider the criterion  $Q$  that is described by [9] and [8] as a tool to predict the influence of the rotation on Horizontal Convection. This criterion consists in the square of the ratio between the thermal boundary layer depth without rotation  $\delta_0 \approx L Ra^{-\frac{1}{5}}$  and the Ekman layer with rotation  $\delta_E \approx L Ek^{\frac{1}{2}}$ . Thus,  $Q = \frac{\delta_0}{\delta_E} \approx \frac{1}{Ra^{-2/5} Ek}$ .

We have to be careful here, as the Ekman number considered in the  $Q$  criterion is the Ekman number based on horizontal length, i.e. defined as  $Ek_{hor} = \frac{Ek}{\Gamma^2}$ . Likewise, we have to take  $Ra_L$  and not  $Ra_F$  for the calculation. This criterion, defined in these articles for high Prandtl number which we do not have, predicts the rotation being extreme for  $Q \gg Ra^{4/15}$ , strong for  $1 \ll Q \ll Ra^{4/15}$  and weak for  $Q \ll 1$ .

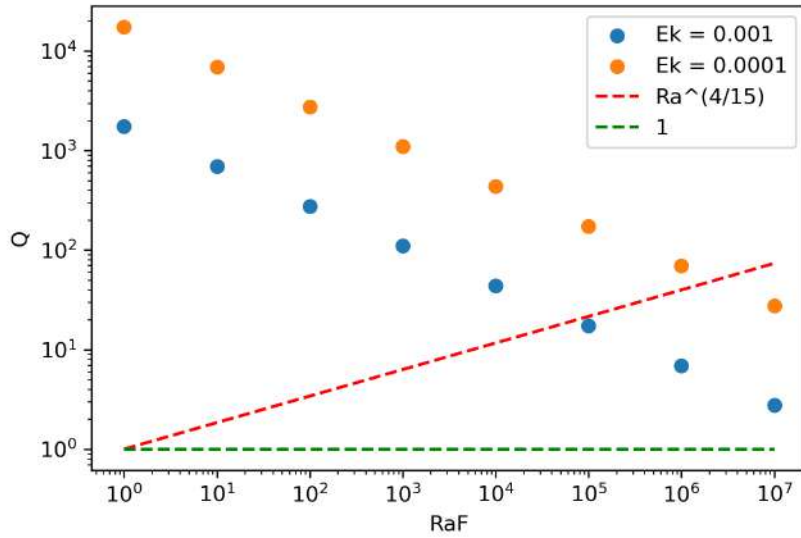


Figure 23: Evolution of the criterion  $Q$  with the Rayleigh number  $Ra_F$  and the Ekman number  $Ek$ .

We show  $Q$  for our simulations in figure 23. We can see that for  $Ra_F = 10^7$ , for both  $Ek = 10^{-4}$  and  $Ek = 10^{-3}$  the rotation is strong. But  $Ek = 10^{-3}$  is approaching  $Q = 1$ , which means that the rotation may be weak, whereas for  $Ek = 10^{-4}$  we are near the frontier to extreme rotation, therefore the flow is still significantly affected by rotation.

## 5 Competition between rotating Rayleigh-Bénard and Horizontal convection

From the beginning our purpose is to study the competition between Rayleigh-Bénard convection and Horizontal Convection. To do so, we will start from the Rayleigh-Bénard convection and gradually add a temperature gradient at the top of the domain, until Horizontal Convection clearly dominates. Then we will use all the diagnostics we have developed so far to determine where the transition from the Rayleigh-Bénard convection to Horizontal Convection occurs.

Now that we have established the behaviour of pure Rayleigh-Bénard Convection and Horizontal Convection, the extreme cases, with two of our entry parameters, the Ekman number and the Rayleigh number, we can decide which parameters to use to vary our third parameter:  $\Lambda$ . Ideally, we want to study all the possibility, that is to say:

- From rotation affected Rayleigh-Bénard to rotation affected Horizontal Convection
- From rotation affected Rayleigh-Bénard to rotation unaffected Horizontal Convection
- From rotation unaffected Rayleigh-Bénard to rotation affected Horizontal Convection
- From rotation unaffected Rayleigh-Bénard to rotation unaffected Horizontal Convection

The choice is easy for the latter, we just have to discard rotation from our simulations, and to take a Rayleigh number high enough so that the convection is fully developed. The choice is a little more complicated for the other transition. First, the HC is more affected by the rotation, so we will not be able to study the transition from a rotation affected RB to rotation unaffected HC in our conditions.

For the other transitions, our options are limited by the necessity to have a Rayleigh number high enough so that we are either rotation-unaffected or supercritical enough for the RB convection but still affected by the rotation for the HC. To be affected by the rotation during the entire transition, we will use  $Ek = 10^{-4}$  that has the largest rotation affected RB regime, and to go from rotation unaffected RB to rotation affected HC  $Ek = 10^{-3}$ .

With these parameters, the most reasonable Rayleigh number is  $Ra_F = 10^7$ . We can see on figure 17 that it seems that the Horizontal Convection has already reached a rotation unaffected regime for these values ( $Ra_F = 10^7$ ,  $\Lambda = 1$  and thus  $Ra_L = 2,56 \cdot 10^9$  for  $Ek = 10^{-3}$  and  $Ek = 10^{-4}$ ). It is true, but for  $\Lambda = 0.1$ ,  $Ra_L = 2,56 \cdot 10^8$ , and rotation effects may be obtained. Since the transition is expected well before  $\Lambda = 1$  ( $\Lambda = 0.01$  based on 2D simulations by [1]), it means that HC may be affected by rotation when it takes over RB convection (strongly affected for  $Ek = 10^{-4}$  and weakly affected for  $Ek = 10^{-3}$  as desired).

### 5.1 Evolution of the Nusselt numbers

The first diagnostic that we will use is the Nusselt number. As we have seen previously, the Nusselt number is a commonly used diagnostic in the literature. Of course we do not expect the Nusselt number corresponding to the dominated convection type to be zero, but to have values small enough compared to the dominating one so that we can decide which dynamics dominate.

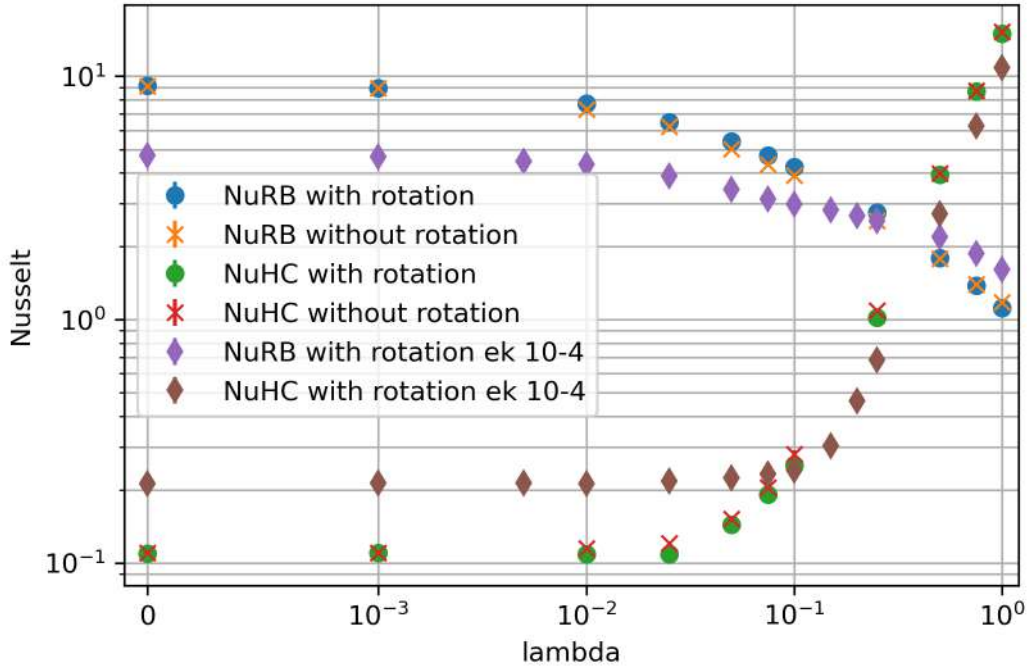


Figure 24: Evolution of the Nusselt number with  $\Lambda$  for different Ekman numbers  $Ek$  from Rayleigh-Bénard convection to Horizontal Convection. With rotation means  $Ek = 10^{-3}$  and without rotation  $Ek = \infty$ .

On figure 24 we can see that we have an excellent fit between  $Ek = 10^{-3}$  and  $Ek = \infty$ . This result is not surprising since we have seen before that with  $Ek = 10^{-3}$  and  $Ra_F = 10^7$  we are in the rotation unaffected for both the RB and the HC. However, we also know that there should be an effect of rotation for  $\Lambda < 1$  and  $Ek = 10^{-3}$  and therefore it could have influenced transition. Especially since we have also seen that these two flows do not look like each other and we could have expected different behaviour as we increase the temperature gradient at the top of the box. We can interpret this result as the fact that the effect of rotation on the Nusselt number is not noticeable as we will be able to see it in the section 5.3. Nevertheless, if we look closely it happens a little earlier for  $Ek = \infty$ , because for  $10^{-2} \leq \Lambda \leq 10^{-1}$ , the  $Nu_{HC}$  is slightly greater for  $Ek = \infty$ , and  $Nu_{RB}$  slightly smaller.

The effect of rotation is much more visible for  $Ek = 10^{-4}$ . As  $Nu_{HC}$  starts to increase for  $\Lambda \geq 2,5 \cdot 10^{-2}$  for  $Ek = 10^{-3}$  or  $Ek = \infty$ , it starts to increase only for  $\Lambda \geq 7,5 \cdot 10^{-2}$  for  $Ek = 10^{-4}$ . It is confirmed by the decrease in  $Nu_{RB}$  that also starts earlier for  $Ek = 10^{-3}$  and  $Ek = \infty$ . These observations indicate that the rotation tends to delays the transition from Rayleigh-Bénard to Horizontal Convection. But, the Nusselt numbers only describing the heat transfer aspect of the problem, we will also look at the other parameters to confirm this first conclusion.

## 5.2 Evolution of the temperature profile

To complement the information given by the Nusselt number, we can look at the temperature profile. Indeed, it gives us information on the thermal organization of our box, and since RB and HC have completely different structures, it will help us identify the transition.

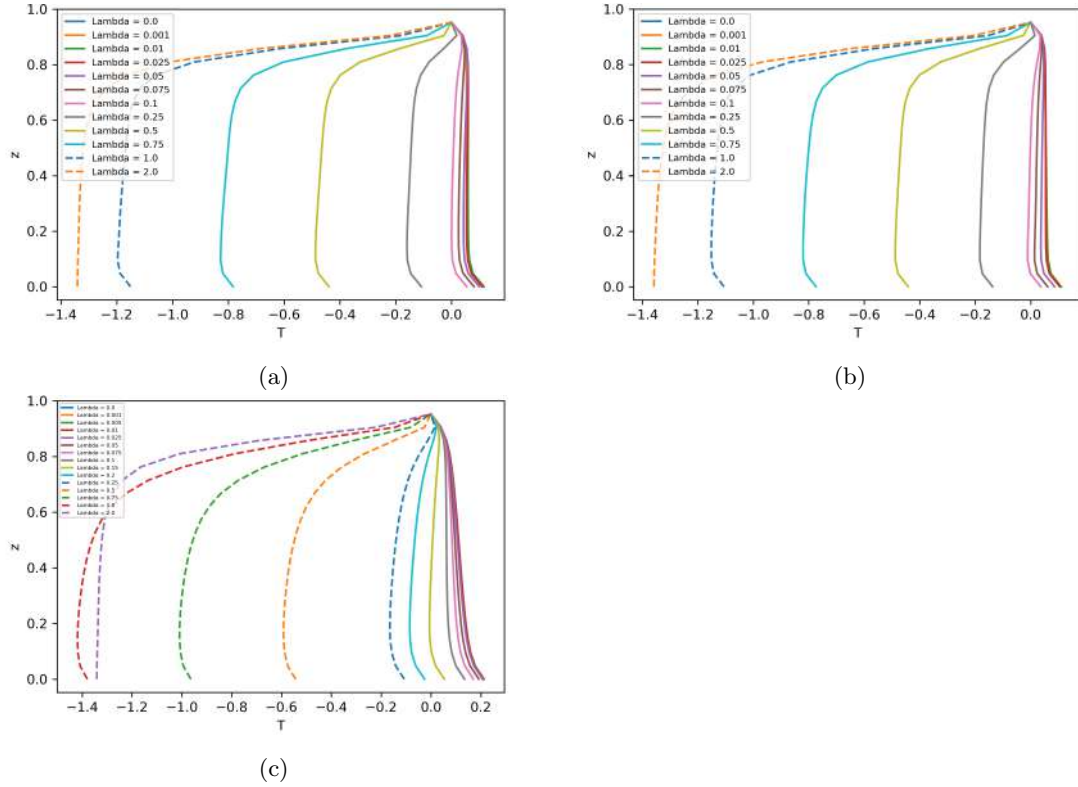


Figure 25: Evolution of the temperature profiles with  $\Lambda$  for different Ekman numbers  $Ek$  at  $Ra_F = 10^7$  from Rayleigh-Bénard convection to Horizontal Convection. The dashed lines are here to differentiate two lines with the same color. (a)  $Ek = \infty$  (b)  $Ek = 10^{-3}$  (c)  $Ek = 10^{-4}$ .

First, we can notice that we do not have the exact horizontal Convection temperature profile as long as there is a flux at the bottom of the domain. It can be seen by looking at the temperature gradient between  $z = 0$  and  $z = 0.1$ . In fully developed Horizontal Convection, we have a perfectly homogeneous bottom, but with Rayleigh-Bénard convection added, the layer is slightly destabilized. It seems almost insignificant when looking at the temperature profile, but it greatly influences the circulation of the fluid as we will see later.

On figures 25a and 25b we can see that we go from a Rayleigh-Bénard temperature profile to a Horizontal Convection one for  $\Lambda \approx 0.075$ , as the temperature gradient inverts itself and the layer at  $z = 0.8$  is colder than the one at  $z = 0.9$ . On figure 25c, this transformation only occurs for  $\Lambda = 0.15$  and is clearly seen for  $\Lambda = 0.2$ .

Therefore, the transition between RB and HC, according to temperature profiles, seems to be delayed by the presence of rotation, as we have already determined with the Nusselt numbers.

### 5.3 Evolution of the Reynolds numbers

The study of the Reynolds number is very interesting, notably because it is a good complement to the Nusselt numbers, since it is not related to the heat transfer properties of the fluid but solely its organization and circulation.

On figure 26a we can clearly see the effect of rotation on the transition between Rayleigh-Bénard convection and Horizontal Convection. Indeed, we have a plateau for low and high  $\Lambda$ , which is approximately the same for  $Ek = \infty$  and  $Ek = 10^{-3}$ ,  $Re_{hor} \approx 70\%$  and  $Re_{hor} \approx 90\%$ , but the transition between them is delayed by the rotation. Thus, the transition without rotation is between  $\Lambda = 10^{-3}$  and  $\Lambda = 10^{-2}$ ,  $\Lambda = 10^{-2}$  and  $\Lambda = 5 \cdot 10^{-2}$  for  $Ek = 10^{-3}$  and  $\Lambda = 2, 5 \cdot 10^{-2}$  and  $\Lambda = 5 \cdot 10^{-1}$  for  $Ek = 10^{-4}$ .

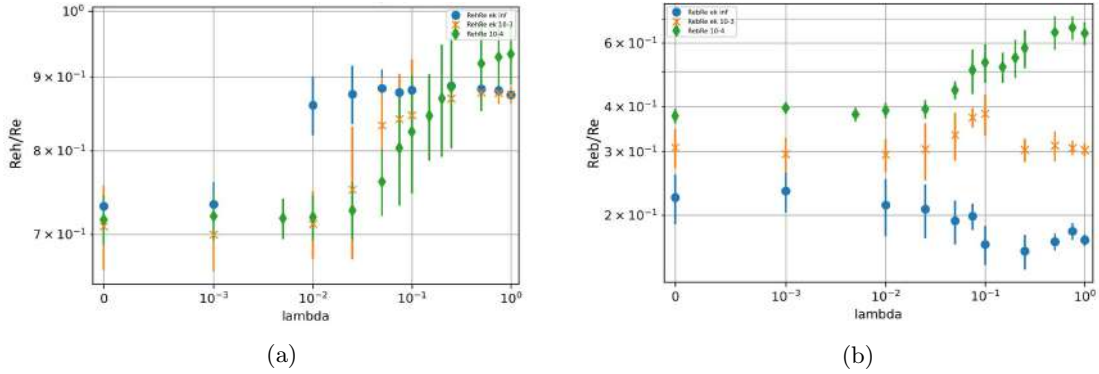


Figure 26: (a) Evolution of the barotropic Reynolds number  $Re_b$  with  $\Lambda$  for  $Ek = \infty$ ,  $Ek = 10^{-3}$  and  $Ek = 10^{-4}$  at  $Ra_F = 10^7$  for transitions from Rayleigh-Bénard convection to Horizontal Convection (b) Evolution of the horizontal Reynolds number  $Re_h$  with  $\Lambda$  for  $Ek = \infty$ ,  $Ek = 10^{-3}$  and  $Ek = 10^{-4}$  at  $Ra_F = 10^7$  for transitions from Rayleigh-Bénard convection to Horizontal Convection. The vertical bars correspond to the temporal standard deviation of the variable.

Figure 26b is also very interesting because it addresses the importance of rotation for the different flows as well as the transition. First of all we can notice that the Ekman number has a direct influence on the barotropic Reynolds number: for all  $\Lambda$  we have  $Re_b(Ek = \infty) \leq Re_b(Ek = 10^{-3}) \leq Re_b(Ek = 10^{-4})$ . As for the horizontal Reynolds number, we have a plateau for low and high  $\Lambda$ : 20% to 15%, 30% to 30% and 38% to 65% for  $Ek = \infty$ ,  $Ek = 10^{-3}$  and  $Ek = 10^{-4}$  respectively. And the transition between these plateaus are also affected by the rotation. It starts to diminish slightly between  $\Lambda = 10^{-3}$  and  $\Lambda = 10^{-2}$  for  $Ek = \infty$  but increases only for  $\Lambda \geq 2, 5 \cdot 10^{-2}$   $Ek = 10^{-3}$  and  $Ek = 10^{-4}$ : the transition is delayed by the rotation.

We also have to note the bump between  $\Lambda = 2, 5 \cdot 10^{-2}$  and  $\Lambda = 2, 5 \cdot 10^{-1}$  for  $Ek = 10^{-3}$ . This can be explained by the fact that as  $\Lambda$  increases  $Ra_L$  increases, such that rotation effects on HC dynamics weaken as we sweep in  $\Lambda$ . Therefore, even if for  $\Lambda = 1$  we are in a rotation unaffected regime, we go through a rotation affected regime before reaching it, and this is what we see here: it appears as an increase in barotropic Reynolds when we go through it as HC already dominates the dynamics. That being said overall the Reynolds number confirms our first conclusion of a delayed transition with the rotation.

## 5.4 Visualization

To conclude, we can look at the organization of the flow during the transition from Rayleigh-Bénard convection to Horizontal Convection with and without rotation. Of course, the transition is continuous and we can not show every increment of  $\Lambda$ , but we can first look at the flow for  $\Lambda = 10^{-3}$  and  $\Lambda = 1$ , the flow being respectively heavily Rayleigh-Bénard convection dominated

and Horizontal Convection dominated. Then to compare the transitions we can look at  $\Lambda = 10^{-2}$  and  $\Lambda = 10^{-1}$ , which correspond to the values at which the transition is made.

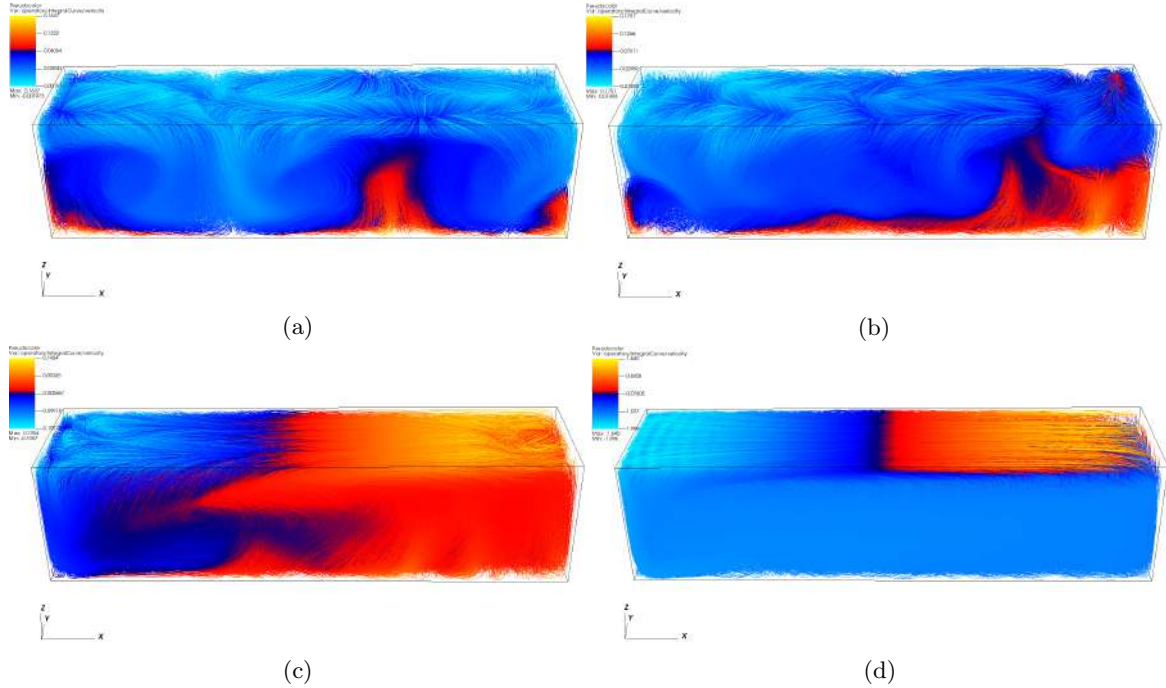


Figure 27: Snapshot of the streamlines of mixed Rayleigh-Bénard and Horizontal Convection simulations without rotation (i.e.  $Ek = \infty$ ), at  $Ra_F = 10^7$ , colored by the temperature, taken at the end of the simulations. (a)  $\Lambda = 10^{-3}$  (b)  $\Lambda = 10^{-2}$  (c)  $\Lambda = 10^{-1}$  (d)  $\Lambda = 1$ .

On figure 27, we can see the transition between Rayleigh-Bénard convection and Horizontal Convection without rotation ( $Ek = \infty$ ), as has been studied by [1]. We can clearly see that the RB convection is not really affected by the slight temperature gradient at the top of the box on figure 27a, maybe with the exception of the little hot plume at the bottom right corner. In the same way, the horizontal Convection does not seem affected by the heat flux at the bottom of the box, when looking at the temperature on figure 27d.

But if we compare the horizontal velocity in the pure HC case (figure 8b) and the  $\Lambda = 1$  case (figure 28), we can see a clear difference. In the second case, the cold layer is disturbed by the geothermal flux at the bottom of the domain (as can be seen on figure 25c). The consequence is that the plume can entirely go through the depth of the box and thus does not create an intrusion.

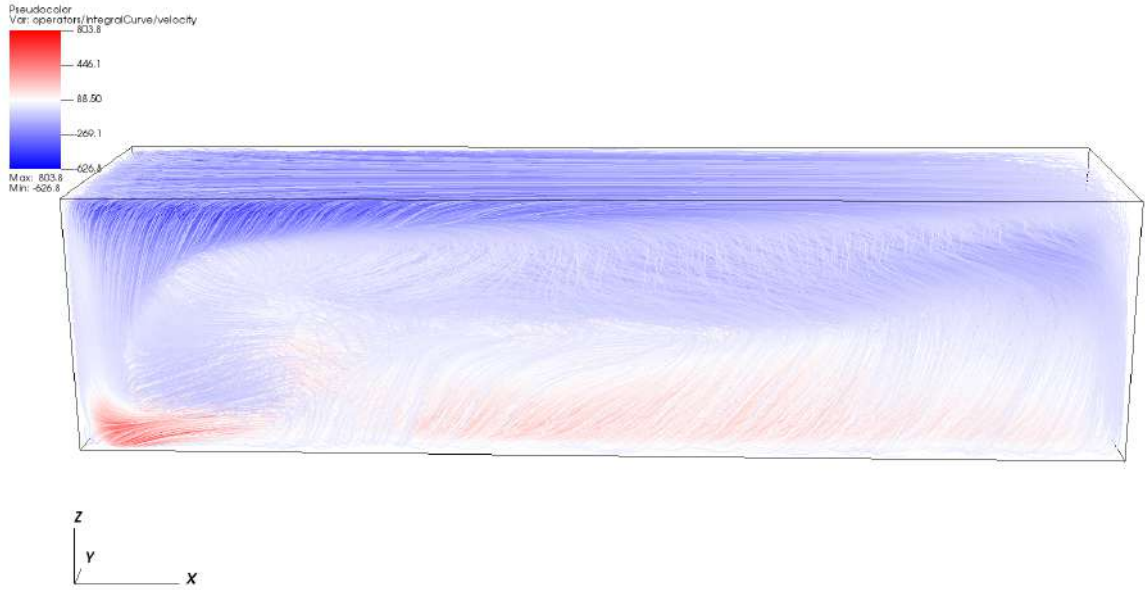


Figure 28: Snapshot of the streamlines of mixed Rayleigh-Bénard and Horizontal convection simulations ( $\Lambda = 1$ ) without rotation (i.e.  $Ek = \infty$ ) for  $Ra_F = 10^7$ , colored by the velocity along the x-axis, taken at the end of the simulations.

On figure 27b, for  $\Lambda = 0.01$ , we can see that the bottom flux is still the main heating source, as the bottom of the domain is hotter than its top right. Thus, the Rayleigh-Bénard convection is still driving the convection, but is greatly disturbed by the top temperature gradient, the heat going up almost exclusively on the right of the domain.

Then, for  $\Lambda = 0.1$ , we can see that Horizontal Convection and Rayleigh-Bénard convection have approximately the same heating strength, the top and bottom of the domain are at the same temperature. It results in a great spatial separation between the x positive and x negative in temperature difference, that reach the entire depth of the box, and not just a thin layer as can be seen on figure 27d.

The fact that  $Ra_L$  is smaller must also be taken into account, as it plays a role in the height of the top layer, but if we compare figure 27c to figure 7c (pure HC with  $Ra_F = 10^5$ ) we can see that it is deeper than what we can expect in a pure HC case. As seen with previous diagnostics, we are at the pivot of the transition.

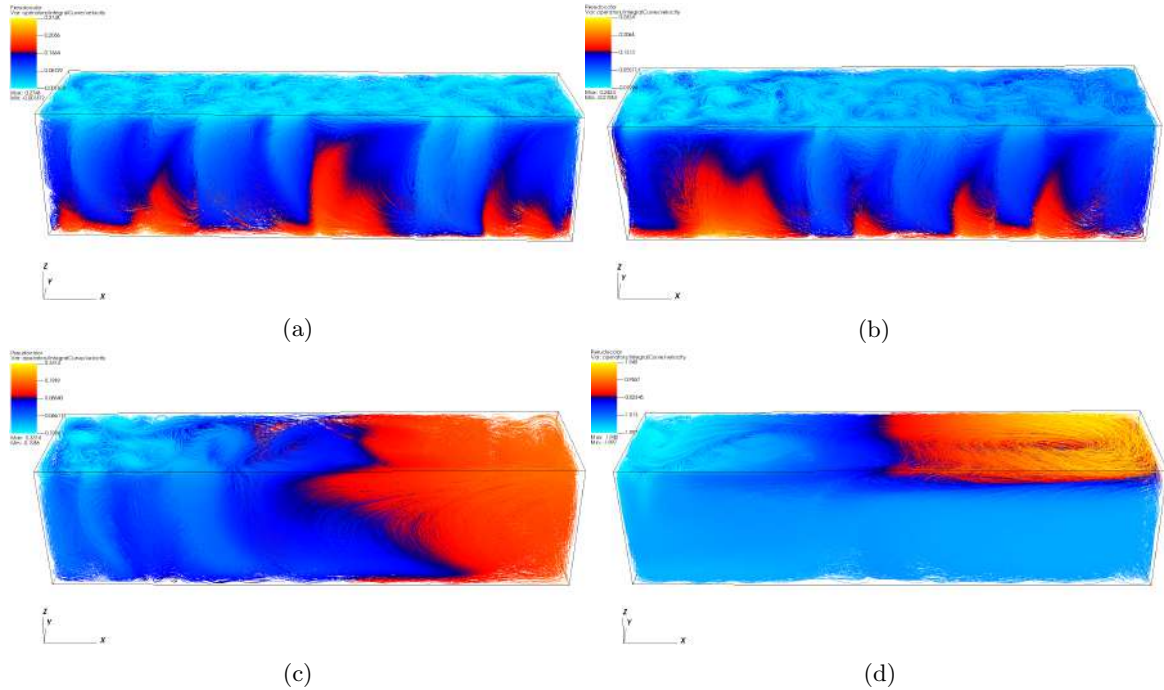


Figure 29: Snapshot of the streamlines of mixed Rayleigh-Bénard and Horizontal Convection simulations with rotation ( $Ek = 10^{-4}$ ), at  $Ra_F = 10^7$ , colored by the temperature, taken at the end of the simulations. (a)  $\Lambda = 10^{-3}$  (b)  $\Lambda = 10^{-2}$  (c)  $\Lambda = 10^{-1}$  (d)  $\Lambda = 1$ .

On figure 29, we can see the transition from rotating Rayleigh-Bénard convection to rotating Horizontal convection. As for figure 27 without rotation, we can see that for  $\Lambda = 10^{-3}$  and  $\Lambda = 1$ , we have clearly a dominating convection without influence of the other heat source, even though the remark concerning the cold layer made for figure 27d also applies for figure 29d.

But contrary to the non-rotating case on figure 27b, here with  $\Lambda = 10^{-2}$  we can see that the flow structure is still only very slightly affected. On figure 29c with  $\Lambda = 10^{-1}$  the flow is clearly influenced by the temperature gradient at the top of the box, which seems to have the same heating influence as the heat flux at the bottom of the box. Nevertheless, the organization in vertical vortices is still present, and could be a cause for this temperature difference between the positive and negative  $x$ , comparable to the one observed on figure 27c.

Overall it appears clearly that the transition without rotation takes place between  $\Lambda = 10^{-2}$  and  $\Lambda = 10^{-1}$  whereas with  $Ek = 10^{-4}$  it has not yet started for  $\Lambda = 10^{-2}$  and we do not have the great convective roll of Horizontal Convection for  $\Lambda = 10^{-1}$ . Therefore, by looking at the flow we can confirm what we had concluded with the other diagnostics, that is to say the rotation delays the transition for Rayleigh-Bénard convection to Horizontal Convection.

## 6 Conclusion

### 6.1 Effect of rotation on the transition

We have seen that our simulations in three dimensions, with no-slip boundary conditions, are in good agreement with what can be found in the literature about rotating and non-rotating Rayleigh-Bénard convection and Horizontal Convection. Using the Nusselt and Reynolds number, as well as visualizations of the simulations, we have been able to determine the parameters for the different regimes, diffusion or convection dominated, and for the latter we further distinguished the rotation-affected regime and the rotation unaffected regime. Our results showed that the presence of rotation, in rotation-affected regimes, tends to inhibit convection.

We have used these first results to determine the best parameters that were accessible to us for the study of the transition from Rayleigh-Bénard convection to Horizontal Convection under different influences of the rotation. The transition without rotation showed an excellent agreement with the results of [1], whose work is here extended to three dimensions.

Then, the simulations with two different strengths of rotation showed that the rotation tends to delay the transition from Rayleigh-Bénard convection to Horizontal Convection. This result is not surprising, as the preliminary results showed that the Horizontal Convection, which consists in longer movements in the horizontal plane, was more affected by the rotation. Therefore, our results strengthen the conclusion reached by [1]: they could conclude without rotation that the movements in subglacial lakes where  $\Lambda = 10^{-3}$  are likely dominated by Rayleigh-Bénard convection, since the transition takes place between  $\Lambda = 10^{-2}$  and  $\Lambda = 10^{-1}$ . The rotation delaying the transition according to our results strengthens this conclusion.

### 6.2 Possible further research

The problem that we are considering has many parameters, some of them are interconnected, and we had to choose which variables to fix, which to vary, and which to let vary as product of others. In a first approach of the subject, setting the aspect ratio, the Prandtl number and the heat flux as constants allowed us to concentrate on the Rayleigh "flux" number, the Ekman number and the parameter  $\Lambda$ . But to be thorough it could be interesting to investigate the effect of the other parameters.

First of all, the effect of the aspect ratio, and overall dimensions of our domain, could be of great interest, as researched by [12] and [11] for HC and RB respectively. Not only are we far from realistic aspect ratios (for simplification purposes), having an aspect ratio of 4 between the x and z dimensions whereas it is close to 100 in reality, but it has showed some influence on the results. In particular the depth of the domain plays a role in the return flow in Horizontal Convection, the cold plume still hitting the bottom at high Rayleigh number.

The aspect ratio between the y and the x dimension could also be interesting to study. Indeed, we can clearly see on the simulations that the rotation creates large vortices for the Horizontal Convection. The question is whether the domain we have considered here is large enough for these vortices to develop. If not, it could inhibit the rotation and thus diminish its effect on the flow. An inhibition that may not exist in reality, as the lakes can be much wider.

Then, in our simulations when we want to study a transition we vary the parameter  $\Lambda$  for a fixed  $Ra_F$ . Since  $Ra_L = Ra_F \Lambda^4$ , it means that we actually vary the Rayleigh number of Horizontal Convection for a fixed Rayleigh-Bénard convection, an effect that can particularly be seen on figure 26b. A great complement to this approach, to be thorough, would be to simulate transition from Horizontal Convection to Rayleigh-Bénard convection, that is to say at a fixed  $Ra_L$ , to verify if it has an influence on the transition.

Finally, we have seen that as we add rotation, the flow structures itself in vortices, with varying diameter and depth, even in rotation unaffected regimes. It could be particularly interesting to study the size and density of these vortices, as Rayleigh-Bénard convection seems to create numerous small ones, and Horizontal Convection fewer but larger ones. This diagnostic could help refine our understanding of the transition and give a more precise value of the  $\Lambda$  at which it occurs.

## References

- [1] Louis-Alexandre Couston, Joseph Nandaha, and Benjamin Favier. Competition between rayleigh–bénard and horizontal convection. *Journal of Fluid Mechanics*, 947:A13, 2022.
- [2] S. Chandrasekhar. *Hydrodynamic and hydromagnetic stability*. Dover Publications, New York, dover ed edition, 1981.
- [3] Guenter Ahlers, Siegfried Grossmann, and Detlef Lohse. Heat transfer and large scale dynamics in turbulent Rayleigh–Bénard convection. *Reviews of Modern Physics*, 81(2):503–537, April 2009.
- [4] Rudie P. J. Kunnen. The geostrophic regime of rapidly rotating turbulent convection. *Journal of Turbulence*, 22(4-5):267–296, May 2021.
- [5] E. M. King, S. Stellmach, and J. M. Aurnou. Heat transfer by rapidly rotating Rayleigh–Bénard convection. *Journal of Fluid Mechanics*, 691:568–582, January 2012.
- [6] Benjamin Favier and Edgar Knobloch. Robust wall states in rapidly rotating rayleigh–bénard convection. *Journal of Fluid Mechanics*, 895:R1, 2020.
- [7] Lister Chiu-Webster, Hinch. Very viscous horizontal convection. *Journal of Fluid Mechanics*, 611(2):395–426, May 2008.
- [8] Wisam K. Hussam, Tze K. Tsai, and Gregory J. Sheard. The effect of rotation on radial horizontal convection and Nusselt number scaling in a cylindrical container. *International Journal of Heat and Mass Transfer*, 77:46–59, October 2014.
- [9] Bishakdatta Gayen and Ross W. Griffiths. Rotating Horizontal Convection. *Annual Review of Fluid Mechanics*, 54(1):105–132, January 2022.
- [10] Kai Leong Chong and Ke-Qing Xia. Exploring the severely confined regime in Rayleigh–Bénard convection. *Journal of Fluid Mechanics*, 805:R4, October 2016.
- [11] Olga Shishkina. Rayleigh–bénard convection: The container shape matters. *Phys. Rev. Fluids*, 6:090502, Sep 2021.
- [12] Gregory J. Sheard and Martin P. King. Horizontal convection: Effect of aspect ratio on Rayleigh number scaling and stability. *Applied Mathematical Modelling*, 35(4):1647–1655, April 2011.

## A Effect of the Prandtl number

For our study, it was particularly important that we had access to different regime of convection and that those existed on a large enough range of Rayleigh number  $Ra_F$ . According to [4], the Prandtl number had an important role in that regard. The article makes the distinction between  $Pr \leq 2$  and  $Pr \geq 2$ , the rotation affected regime existing for a larger Rayleigh number range in the second case. To choose the right input parameters for our simulations, we compared the effect of the Prandtl number on the scaling of the Nusselt number  $Nu_{RB}$  with the Rayleigh number  $Ra_F$ .

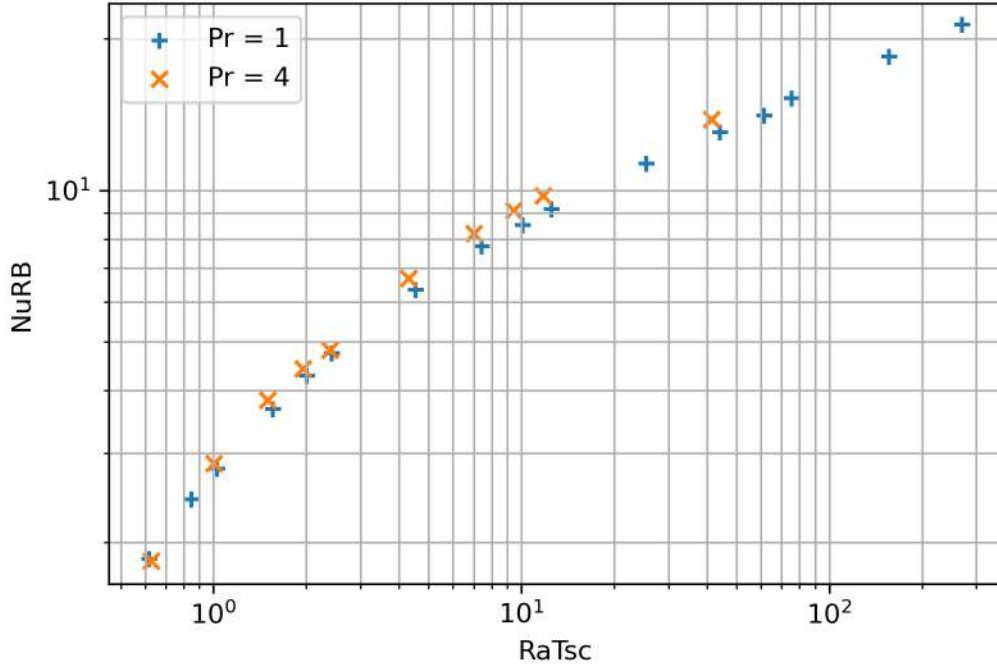


Figure 30: Evolution of the Nusselt number  $Nu_{RB}$  with the supercritical Rayleigh number  $Ra_T/Ra_c(Ek, Pr)$  for two different Prandtl numbers  $Pr = 1$  and  $Pr = 4$  at  $Ek = 10^{-3}$ .

On figure 30 we can see that a higher Prandtl number, although it increases the difficulty of computation, does not have much impact on the effect of rotation on the Nusselt number. Therefore, we used  $Pr = 1$  in our simulations.

## B Dimensionless numbers

One of the difficulty of this study is that we combine two well-known different problems that use the same dimensionless numbers, but defined with slight differences due to the configurations differences. Therefore, it is necessary that we define those dimensionless numbers properly to avoid errors.

The convention that we will use here are:

$$\left\{ \begin{array}{l}
\text{Thermal expansion coefficient} = \alpha \\
\text{Kinetic viscosity} = \nu \\
\text{thermal diffusivity of fluid} = \kappa \\
\text{Rotation Rate} = \Omega \\
\text{Total heat flux} = F \\
\text{Thermal conductivity of fluid} = k \\
\text{Vertical length} = H \\
\text{Horizontal length} = L \\
\text{Vertical temperature difference} = \Delta T \\
\text{Horizontal temperature difference} = \Delta T_{hor} \\
\text{Aspect ratio} = \frac{L}{H} = \Gamma.
\end{array} \right. \quad (40)$$

## B.1 Rayleigh numbers

First we have a critical input number, the Rayleigh number, that is defined differently depending on the problem, Rayleigh-bénard convection or horizontal convection, and depending on the imposed boundary conditions, that can be either temperature or fluxes or a combination of both.

The usual set-up for Rayleigh-Bénard convection is with temperature imposed, So we will use this definition of the Rayleigh number:

$$Ra = \frac{g\alpha\Delta TH^3}{\nu\kappa}.$$

We will call it  $Ra_T$  to differentiate it from other definitions.

For horizontal convection, we will also use the definition of the Rayleigh number based on temperature difference:

$$Ra = \frac{g\alpha\Delta T_{hor}L^3}{\nu\kappa}.$$

We will call it  $Ra_L$  to differentiate it from other definitions.

We have to compare these two Rayleigh numbers with the one that we will use in our simulations, so that we can confront our results with the literature. Since we are imposing the flux at the bottom of our box, we cannot use the typical Rayleigh number for Rayleigh-Bénard convection. Instead, we use this definition of the Rayleigh number:  $Ra = \frac{g\alpha FH^4}{k\nu\kappa}$

We will call it  $Ra_F$ .

To link  $Ra_F$  to  $Ra_L$ , we can use  $\Lambda = \frac{k\Delta T_{hor}}{FL}$ .

$$Ra_L = \frac{g\alpha\Delta T_{hor}L^3}{\nu\kappa} = \frac{gFL^4}{k\nu\kappa} \frac{\Delta T_{hor}k}{FL} = \frac{g\alpha FH^4}{k\nu\kappa} \Lambda \left(\frac{L}{H}\right)^4 = Ra_F \Lambda \Gamma^4.$$

To link  $Ra_F$  to  $Ra_T$ , we can use  $Nu_{RB} = \frac{FH}{k\langle T(z=0) \rangle_{xy} - \min(T)}$ .

$$Ra_T = \frac{g\alpha\Delta TH^3}{\nu\kappa} = \frac{g\alpha FH^4}{k\nu\kappa} \frac{k\Delta T}{FH} = \frac{Ra_F}{Nu_{RB}}.$$

$$\text{To sum up: } \mathbf{Ra}_F = \mathbf{Nu}_{RB} \mathbf{Ra}_T = \frac{\mathbf{Ra}_F}{\Gamma^4 \Lambda}.$$

## B.2 Ekman numbers

Another input of our simulations is the Ekman number  $Ek = \frac{\nu}{|f|H^2}$ . This number is valid when we want to study a mainly vertical dynamic, like the Rayleigh-Bénard convection. But when we work on mainly horizontal movement, like the horizontal convection, we have to adjust this number. It becomes  $Ek_{hor} = \frac{\nu}{|f|L^2} = \frac{\nu}{|f|H^2} \left(\frac{H}{L}\right)^2 = \frac{Ek}{\Gamma^2}$

$$\mathbf{Ek} = \mathbf{\Gamma}^2 \mathbf{Ek}_{hor}$$

### B.3 Nusselt number

To characterize the state of the flow depending on the parameters, we will calculate the Nusselt numbers of the flow,  $Nu_{RB}$  corresponding to the Nusselt for Rayleigh-Bénard convection, and  $Nu_{HC}$  for the horizontal convection.

$$\begin{cases} Nu_{RB} = \frac{1}{\langle T(z=0) \rangle_{xy} - \min(T)} = \frac{1}{\langle T(z=0) \rangle_{xy} + \frac{\Gamma\Lambda}{2}} \\ Nu_{HC} = \frac{1}{\langle T_{diff}(z=1) \partial_z T_{diff}(z=1) - T_{diff}(z=0) \partial_z T_{diff}(z=0) \rangle_{xy}}. \end{cases} \quad (41)$$

$T_{diff}$ , the temperature in the same condition but without convection, can be calculated analytically.

$$\begin{cases} T_{diff}(x, y, z) = \frac{\Lambda\Gamma \sin(\frac{\pi x}{\Gamma}) \cosh(\frac{\pi z}{\Gamma})}{2 \cosh(\frac{\pi}{\Gamma})} + 1 - z \\ \partial_z T_{diff}(x, y, z) = \frac{\Lambda\pi \sin(\frac{\pi x}{\Gamma}) \sinh(\frac{\pi z}{\Gamma})}{2\pi \cosh(\frac{\pi}{\Gamma})} - 1 \end{cases} \quad (42)$$

$$\begin{cases} T_{diff}(x, y, 0) = \frac{\Lambda\Gamma \sin(\frac{\pi x}{\Gamma})}{2 \cosh(\frac{\pi}{\Gamma})} + 1 \\ \partial_z T_{diff}(x, y, 0) = -1 \\ T_{diff}(x, y, 1) = \frac{\Lambda\Gamma}{2} \sin(\frac{\pi x}{\Gamma}) \\ \partial_z T_{diff}(x, y, 1) = \frac{\Lambda\pi}{2} \sin(\frac{\pi x}{\Gamma}) \tanh(\frac{\pi}{\Gamma}) - 1 \\ T_{diff}(z=1) \partial_z T_{diff}(z=1) - T_{diff}(z=0) \partial_z T_{diff}(z=0) = (\frac{\Lambda\Gamma}{2} \sin(\frac{\pi x}{\Gamma})) (\frac{\Lambda\pi}{2} \sin(\frac{\pi x}{\Gamma}) \tanh(\frac{\pi}{\Gamma}) - 1 + \frac{1}{\cosh(\frac{\pi}{\Gamma})}) + 1 \\ \langle T_{diff}(z=1) \partial_z T_{diff}(z=1) - T_{diff}(z=0) \partial_z T_{diff}(z=0) \rangle_{xy} = 1 + \frac{\Lambda^2 \Gamma \pi}{8} \tanh(\frac{\pi}{\Gamma}). \end{cases} \quad (43)$$